POLITECNICO DI TORINO
Repository ISTITUZIONALE

Ambient groundwater flow diminishes nitrate processing in the hyporheic zone of streams

Original
Ambient groundwater flow diminishes nitrate processing in the hyporheic zone of streams / Azizian, Morvarid; Boano, Fulvio; Cook, Perran L. M.; Detwiler, Russell L.; Rippy, Megan A.; Grant, Stanley B.. - In: WATER RESOURCES RESEARCH. - ISSN 0043-1397. - ELETTRONICO. - 53:5(2017), pp. 3941-3967. [10.1002/2016WR020048]

Availability:
This version is available at: 11583/2675304 since: 2021-03-29T19:56:20Z

Publisher:
American Geophysical Union

Published
DOI:10.1002/2016WR020048

Terms of use:

This article is made available under terms and conditions as specified in the corresponding bibliographic description in the repository

Publisher copyright
AGU

Da definire

(Article begins on next page)

12 October 2024

AGU PUBLICATIONS

Water Resources Research

RESEARCH ARTICLE

10.1002/2016WR020048

Special Section:
Emergent Aquatic Carbon-nutrient Dynamics as Products of Hydrological, Biogeochemical, and Ecological Interactions

Ambient groundwater flow diminishes nitrate processing in the hyporheic zone of streams

Morvarid Azizian[1], Fulvio Boano[2], Perran L. M. Cook[3], Russell L. Detwiler[4], Megan A. Rippy[4], and Stanley B. Grant[1,4]

[1]Department of Chemical Engineering and Materials Science, Henry Samueli School of Engineering, University of California, Irvine, California, USA, [2]Department of Environment, Land and Infrastructure Engineering, Politecnico di Torino, Torino, Italy, [3]Water Studies Centre, School of Chemistry, Monash University, Clayton, Victoria, Australia, [4]Department of Civil and Environmental Engineering, Henry Samueli School of Engineering, University of California, Irvine, California, USA

Key Points:
- Nitrate uptake velocities are simulated using a modeling framework that accounts for hyporheic exchange and ambient groundwater flow
- Fluvial ripples dominate hyporheic exchange flux, but riffle-pool sequences dominate the turnover of nitrate and ammonium in streambed sediments
- The Damköhler Number and hyporheic exchange flux are primary controls on N-cycling, but both are influenced by ambient groundwater flow

Supporting Information:
- Supporting Information S1
- Software S1–S3

Correspondence to:
S. B. Grant,
sbgrant@uci.edu

Citation:
Azizian, M., F. Boano, P. L. M. Cook, R. L. Detwiler, M. A. Rippy, and S. B. Grant (2017), Ambient groundwater flow diminishes nitrate processing in the hyporheic zone of streams, *Water Resour. Res.*, *53*, 3941–3967, doi:10.1002/2016WR020048.

Received 2 NOV 2016
Accepted 29 MAR 2017
Accepted article online 11 APR 2017
Published online 15 MAY 2017

© 2017. American Geophysical Union. All Rights Reserved.

Abstract Modeling and experimental studies demonstrate that ambient groundwater reduces hyporheic exchange, but the implications of this observation for stream N-cycling is not yet clear. Here we utilize a simple process-based model (the Pumping and Streamline Segregation or PASS model) to evaluate N-cycling over two scales of hyporheic exchange (fluvial ripples and riffle-pool sequences), ten ambient groundwater and stream flow scenarios (five gaining and losing conditions and two stream discharges), and three biogeochemical settings (identified based on a principal component analysis of previously published measurements in streams throughout the United States). Model-data comparisons indicate that our model provides realistic estimates for direct denitrification of stream nitrate, but overpredicts nitrification and coupled nitrification-denitrification. Riffle-pool sequences are responsible for most of the N-processing, despite the fact that fluvial ripples generate 3–11 times more hyporheic exchange flux. Across all scenarios, hyporheic exchange flux and the Damköhler Number emerge as primary controls on stream N-cycling; the former regulates trafficking of nutrients and oxygen across the sediment-water interface, while the latter quantifies the relative rates of organic carbon mineralization and advective transport in streambed sediments. Vertical groundwater flux modulates both of these master variables in ways that tend to diminish stream N-cycling. Thus, anthropogenic perturbations of ambient groundwater flows (e.g., by urbanization, agricultural activities, groundwater mining, and/or climate change) may compromise some of the key ecosystem services provided by streams.

Plain Language Summary Humans generate vast quantities of bioavailable nitrogen for agricultural production, and much of the excess ends up in rivers and streams. As the nitrogen flows downstream, some of it is naturally removed by streambed sediments through a process known as hyporheic exchange. In this paper, we set out to answer the question: how does the movement of groundwater into (or out of) a stream affect the removal of nitrogen by hyporheic exchange? Multiscale and multi-physics model simulations suggest that groundwater movement across the streambed can "shut down" the physical and biological processes that remove stream nitrogen. Hence, stream-groundwater interactions may play an important role in modulating the human and environmental impacts of nitrogen pollution.

1. Introduction

Humans more than doubled the annual terrestrial input of bioavailable nitrogen over the past century, from 155 Tg N y^{-1} in 1900 to 345 Tg N y^{-1} in 2000 [*Galloway et al.*, 2004; *Seitzinger et al.*, 2006]. This number is projected to increase another 18–48% (from 408 to 510 Tg N y^{-1}) by the year 2030 [*Bouwman et al.*, 2005]. Much of this anthropogenic nitrogen finds its way to rivers and streams through point and nonpoint source pollution, including return flows from irrigated agriculture, runoff from confined animal feeding operations, septic tank leachates, and partially treated municipal wastewater discharges, to name a few [*Jongbloed and Lenis*, 1998; *Carey and Migliaccio*, 2009; *Morée et al.*, 2013]. As nitrate loading increases, streams less efficiently remove nitrate by biological assimilation and denitrification [*Bernot and Dodds*, 2005; *Mulholland et al.*, 2008] and disproportionately more nitrate escapes to downstream receiving waters where it threatens both human and ecosystem health [*Smith et al.*, 1999; *Powlson et al.*, 2008; *Canfield et al.*, 2010]. An alarming

example is currently playing out in the Gulf of Mexico, where nitrate discharged from the Mississippi and Atchafalaya Rivers is responsible, at least in part, for a seasonal hypoxic region (or "dead zone") the size of the U.S. State of Connecticut [*Coppess*, 2016].

As nitrogen is transported downstream upwards of 70% is removed from the stream by biological assimilation and denitrification [*Peterson et al*., 2001; *Galloway et al*., 2004; *Birgand et al*., 2007], and much of this ecosystem service is thought to occur in the hyporheic zone [*Groffman et al*., 2005; *Bohlke et al*., 2009; *Zarnetske et al*., 2011, 2012; *Kiel and Cardenas*, 2014] and riparian zone [*McClain et al*., 2003]. The hyporheic zone is often defined as the portion of the streambed where hydrological flow paths start and terminate at the stream [*Gooseff*, 2010; *Boano et al*., 2014]. The cycling of water, oxygen, and nutrients between the stream and hyporheic zone ("hyporheic exchange") drives a number of biological processes that influence stream water quality, including stream nitrate concentrations [*Huettel et al*., 2014; *Rode et al*., 2015]. Water and solutes are "pumped" into and out of the sediment by static and dynamic pressure variations over the sediment-water interface [*Thibodeaux and Boyle*, 1987; *Grant and Marusic*, 2011; *Boano et al*., 2014]. Water and mass move from the stream to the sediment in high-pressure regions (downwelling zones) and from the sediment to the stream in low-pressure regions (upwelling zones). Hyporheic exchange can also occur due to variations in streambed hydraulic conductivity [*Herzog et al*., 2015], bed form migration [*Rutherford et al*., 1993; *Elliott and Brooks*, 1997a, 1997b; *Ahmerkamp et al*., 2015], and bioirrigation [*Vaughn and Hakenkamp*, 2001; *Meysman et al*., 2006a, 2006b].

The pumping of water through submerged ripples and riffle-pool sequences, in particular, appears to dominate hyporheic exchange fluxes and nutrient turnover in many streams [*Gomez-Velez and Harvey*, 2014; *Gomez-Velez et al*., 2015]. Because hyporheic exchange across ripples and riffle-pool sequences occurs over different time scales (minutes-to-hours versus hours-to-days, respectively) [*Boano et al*., 2014], these two bed form scales could also serve different functional roles relative to N-cycling; e.g., producing nitrate at one scale and consuming nitrate at another, depending on the local balance between transport and respiration rates [*Groffman et al*., 2005; *Zarnetske et al*., 2011, 2012; *Azizian et al*., 2015].

At the reach scale, the net removal (or generation) of stream nitrate can be quantified with the nitrate uptake velocity (v_f, units m s^{-1}), defined here as the flux of nitrate out of the streambed divided by the nitrate concentration in the stream [*Stream Solute Workshop*, 1990; *Wollheim et al*., 2006]. The nitrate uptake velocity is favored over other metrics of nitrate attenuation (e.g., the uptake length scale) [*Peterson et al*., 2001], because it isolates the influence of biological processes on nitrate removal in the streambed [*Wollheim et al*., 2006]. In a review of nitrate pollution in agriculturally impacted streams, *Birgand et al*. [2007] concluded that the uptake velocity "is a powerful concept that should be henceforth commonly used in studies of nitrogen removal" (pg. 469). For the sign convention adopted here, the nitrate uptake velocity is negative (or positive) when the streambed is a sink (or a source) of nitrate, respectively.

There is an urgent need for modeling tools that can provide realistic estimates for the nitrate uptake velocity in support of regulatory, ecological, and sustainability goals, including implementation of total maximum daily loads for nitrogen impaired streams [*French et al*., 2006], stream restoration efforts to improve the retention and removal of bioavailable nitrogen [*Craig et al*., 2008], and long-term forecasts of the effects of land-use and climate change on water resources at the watershed scale [*Grathwohl et al*., 2013]. To this end, several process-based models for v_f have been proposed, but these: (1) do not consider the multiscale nature of hyporheic exchange flows and, in particular, the impact of ambient groundwater flow on hyporheic exchange; (2) rely on simplified conceptualizations of mixing within streambed sediments (e.g., a well-mixed box); (3) neglect important steps in the N-cycle (e.g., nitrification and ammonification); and/or (4) adopt pseudo-first-order kinetic descriptions of denitrification [*Stream Solute Workshop*, 1990; *Runkel*, 2007; *Yang and Wang*, 2010]. The first limitation is particularly concerning given that groundwater resources are increasingly under stress from urbanization, agricultural activities, groundwater mining, and climate change [*Walsh et al*., 2005; *Green et al*., 2011; *Askarizadeh et al*., 2015]. The effects of ambient groundwater flow on in-stream ecosystem services are largely unknown [*Boulton et al*., 2010; *Grathwohl et al*., 2013; *Wondzell*, 2015].

In this paper, we develop and test a simple and scalable process-based model for estimating the nitrate uptake velocity that addresses the limitations identified above. In particular, our model accounts for: (1) hyporheic exchange at multiple scales together with ambient groundwater flow in gaining or losing

streams; (2) the broad residence time distributions characteristic of hyporheic exchange; (3) key biogeochemical reactions associated with N-cycling, including respiration, ammonification, nitrification, and denitrification; and (4) the nonlinear nature of the pertinent biogeochemical reaction rates, including Monod kinetics for aerobic respiration and denitrification, and second-order kinetics for nitrification. Using this modeling framework, we systematically evaluate how changing ambient groundwater flow is likely to affect N-cycling in the hyporheic zone of streams, and compare our predictions to previously published reach-scale measurements of nitrate removal.

The paper is organized as follows. We begin by presenting our modeling framework, which we refer to as the Pumping and Streamline Segregation or PASS model (section 2). Information needed to implement the PASS model is then described, including (1) a biokinetic model for the evolution of nitrate concentration with travel time through the hyporheic zone (section 3); (2) physical models for the hyporheic exchange of water through ripples and riffle-pool sequences (section 4); and (3) physical models for the residence time distributions associated with these two bed form scales (section 5). These results are then combined through the PASS modeling framework to predict nitrate uptake velocities for a variety of scenarios related to stream chemistry, bed form scale, stream discharge, and ambient groundwater flow (section 6). We end with a discussion of how these nitrate uptake velocity predictions might be scaled-up to watersheds (section 7), and model limitations and future directions (section 8).

2. Pumping and Streamline Segregation (PASS) Model for Nitrate Uptake

2.1. PASS Model Formulation

Numerous studies have documented that advection is the dominant mechanism by which mass is exchanged across the sediment-water interface in permeable streambeds, defined as streambeds with permeability $>10^{-12}$ m [*Grant and Marusic*, 2011; *Kessler et al*., 2013a, 2013b; *Boano et al*., 2014; *Huettel et al*., 2014]. Here we conceptualize this advective exchange as flow through a bundle of small diameter tubes (referred to as hyporheic zone tubes or HZTs) that collectively represent the various flow paths stream water takes as it moves through the hyporheic zone (Figure 1). Biogeochemical reactions in the sediment cause nutrient and oxygen concentrations to evolve continuously along the HZTs; e.g., sediment-associated microbial biofilms consume oxygen, causing the oxygen concentration in a water parcel to decline with travel time through the hyporheic zone [*Zarnetske et al*., 2011, 2012; *Kessler et al*., 2013a, 2013b]. As a water parcel exits the HZT and returns to the stream, its final nitrate concentration (denoted here by the function $C_{HZT-NO_3^-}(\tau;\text{"chemistry"})$, units mol m^{-3}) will depend on the water parcel's travel time through the hyporheic zone (τ, units s) conditioned on subsurface biogeochemical reactions that consume and produce nitrate (denoted here by the shorthand "chemistry"). Provided there is no mixing of mass across or within HZTs (i.e., mass transport occurs only by advection through the HZT, discussed further in section 2.2), mass

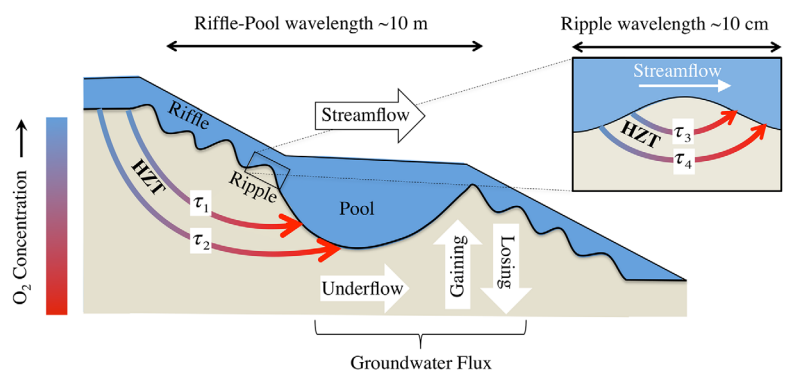

Figure 1. Hyporheic exchange and ambient groundwater flux influence nitrogen cycling in the hyporheic zone of a stream. Here, ambient groundwater flux has both vertical (gaining or losing) and horizontal (underflow) components. Hyporheic zone tubes (HZTs) with different residence times (denoted by the labels τ_1 through τ_4) represent the various flow paths stream water takes as it undergoes hyporheic exchange through submerged bed forms. Two submerged bed form scales are illustrated here: riffle-pool sequences (wavelength ~10 m) and fluvial ripples (wavelength ~10 cm). As water travels through a HZT, microbial respiration of organic carbon consumes oxygen and creates anoxic conditions favorable for denitrification, as indicated by the transition in color from blue to red.

balance over a single submerged and periodic bed form yields the PASS model for nitrate uptake velocity [*Rutherford et al.*, 1993, 1995; *Grant et al.*, 2014; *Azizian et al.*, 2015; *Tonina et al.*, 2015]:

$$v_f = q_H\left[\bar{C}_{HZT-NO_3^-} - 1\right] \tag{1a}$$

$$\bar{C}_{HZT-NO_3^-} = \frac{1}{C_{S-NO_3^-}}\int_0^\infty C_{HZT-NO_3^-}(\tau;\text{“chemistry”})\times E(\tau)d\tau \tag{1b}$$

Variables appearing in these equations include: (1) the volume of stream water pumped through the hyporheic zone per streambed area per time (“hyporheic exchange flux”, q_H, units m s^{-1}); (2) the residence time distribution (RTD) of water in the hyporheic zone $E(\tau)$ (units s^{-1}), where $E(\tau)d\tau$ represents the fraction of hyporheic exchange flux with a HZT travel time within $d\tau$ of τ [*Levenspiel*, 1972; *Hill*, 1977]; (3) the stream nitrate concentration $C_{S-NO_3^-}$ (units mol m^{-3}); and (4) the normalized “breakthrough” concentration of nitrate in an upwelling zone ($\bar{C}_{HZT-NO_3^-}$, unitless). The last quantity is calculated from the ratio of the flow-weighted nitrate concentration returning to the stream in an upwelling zone (integral term in equation (1b)) and the stream nitrate concentration $C_{S-NO_3^-}$ [*Grant et al.*, 2014; *Azizian et al.*, 2015; *McCluskey et al.*, 2016].

To illustrate how the PASS model captures the physics and chemistry of N-cycling in the hyporheic zone, consider the hypothetical example where all water leaving the hyporheic zone has a single residence time, denoted here by the variable τ^*. In this event, the RTD reduces to the Dirac delta function, $E(\tau)=\delta(\tau-\tau^*)$, and the PASS model simplifies:

$$v_f = q_H[F_N(\tau^*) - 1] \tag{2a}$$

$$F_N(\tau^*) = \frac{C_{HZT-NO_3^-}(\tau^*;\text{“chemistry”})}{C_{S-NO_3^-}} \tag{2b}$$

Following *Zarnetske et al.* [2012], the variable F_N represents the fraction of nitrate remaining after a water parcel spends a time τ^* traveling through the hyporheic zone. From equation (2a), we can identify several limits of interest. First, if all nitrate is removed (e.g., by denitrification), then the fraction of nitrate remaining is zero ($F_N=0$). In this “mass transfer limit”, or MTL, nitrate uptake by the streambed depends solely on the hyporheic exchange flux: $v_{f,MTL}=-q_H$. Alternatively, for values of fractional removal less than unity ($0 < F_N \leq 1$), the nitrate uptake velocity depends on the magnitude of both q_H and F_N, a condition we refer to as reaction-limited nitrate uptake. An extreme example is when $F_N=1$, and hyporheic exchange plays no functional role relative to nitrate generation or removal ($v_f=0$). Finally, in sediments that are net nitrifying (i.e., the generation of nitrate by nitrification exceeds the removal of nitrate by other processes, $F_N > 1$), the nitrate uptake velocity will be positive ($v_f > 0$) and its magnitude will depend both on the hyporheic exchange flux q_H and the extent to which the nitrate concentration increases during passage through the hyporheic zone.

Which of these limits apply to a particular stream may depend on the magnitude of the dimensionless Damköhler Number (Da, unitless), defined here as the ratio of the characteristic travel time of water undergoing hyporheic exchange (τ_T) and the timescale for mineralization of organic carbon within the streambed (τ_R): $\mathrm{Da}=\tau_T/\tau_R$. The MTL condition, for example, is most likely to occur when the Damköhler Number is large ($\mathrm{Da} \gg 1$), because long transport timescales together with short mineralization timescales are associated with anaerobic conditions in the sediments and nitrate removal by denitrification [*Boano et al.*, 2010; *Mazadri et al.*, 2011; *Zarnetske et al.*, 2011, 2012; *Kessler et al.*, 2013a, 2013b; *Azizian et al.*, 2015]. On the other hand, for intermediate ($\mathrm{Da} \approx 1$) or small ($\mathrm{Da} \ll 1$) values of the Damköhler Number, the sediments may serve as a reaction-limited sink of nitrate ($-q_H < v_f \leq 0$) or as a net source of nitrate through the nitrification of ammonium ($v_f > 0$) [*Zarnetske et al.*, 2012]. The ammonium, in turn, may be downwelled from the stream or generated in situ by the respiration of sediment organic carbon (i.e., ammonification) [*Cook et al.*, 2006; *Azizian et al.*, 2015]. In practice, hyporheic exchange exhibits a broad range of residence times (not a single residence time, as assumed in the hypothetical example above), and thus the integral form of the nitrate uptake velocity (equation (1)) must be used in place of equation (2).

2.2. The Segregated Streamline Hypothesis

The PASS model assumes that all HZTs are completely segregated; i.e., there is no mixing of mass across or within HZTs. The concept of complete segregation can be traced back to chemical engineering reactor

Table 1. Physical Parameter Values Used for the PASS Model Simulations (Variables Defined in Notation Section)

Parameters (Units)	Value	
Alluvium characteristics		
K_h (m s^{-1})	5×10^{-4}	
S	0.02	
q_U (m s^{-1})	10^{-5}	
q_V (m s^{-1})	0, $\pm5.8\times10^{-6}$, $\pm23\times10^{-6}$	
θ	0.3	
Riffle-pool dimensions		
Period (m)	10	
Amplitude (m)	0.5	
Ripple dimensions		
H (m)	0.02	
λ (m)	0.15	
a	0.16	
m	3/8	
Stream flow characteristics	High stream discharge	Low stream discharge
Q (m^3 s^{-1})	17.47	7.40
d_s (m)	1	0.7
U (m s^{-1})	1.95	1.15

design, where a distinction is made between macromixing and micromixing within a chemical reactor [*Rawlings and Ekerdt*, 2013]. In the present context, macromixing refers to the diversity of flow paths water parcels take as they pass through the hyporheic zone, represented here by the RTD function $E(\tau)$. Micromixing, on the other hand, refers to the exchange of mass between individual water parcels during their residence times, and falls along a spectrum from complete segregation (adopted here) to maximum-mixedness [*Rawlings and Ekerdt*, 2013]. In the complete segregation limit, mixing across HZTs occurs at the last possible moment as water exits the hyporheic zone and returns to the stream. In the maximum mixedness limit, mixing occurs as soon as possible while accounting for the fact that water parcels cannot be mixed for longer than their residence time. A key result of this theory is that the magnitude (and sign) of error introduced by adopting a particular micromixing model depends on the order of the underlying reaction. For example, the micromixing model has no effect on substrate conversion if the underlying reaction is first-order [*Rawlings and Ekerdt*, 2013]. Micromixing can also be thought of in terms of idealized reactors; e.g., the complete segregation limit is equivalent to assuming that a water parcel behaves like a batch reactor as it travels along a HZT. Importantly, different types (and combinations) of idealized reactors can be used to characterize the influence of micromixing on chemical transformations. Elucidating the most appropriate such model for the hyporheic zone is an interesting topic for future study [e.g., see *Feinberg and Hildebrandt*, 1997].

2.3. Stream Bed and Ambient Flow Scenarios

In the analysis presented below, we use the PASS model to estimate the nitrate uptake velocity under a variety of ambient flow conditions. These calculations are carried out assuming that the stream in question has a sandy streambed of constant hydraulic conductivity ($K_h=5\times10^{-4}$ m s^{-1}), mean slope of $S=2\%$, and porosity $\theta=0.3$. Ten ambient flow conditions are evaluated, including two choices of stream discharge ($Q=$ 17.47 m^3 s^{-1} and 7.40 m^3 s^{-1}, denoted "H-Q" and "L-Q," respectively), five choices of vertical groundwater flux ($q_V=$ 0, $\pm5.8\times10^{-6}$, and $\pm2.3\times10^{-5}$ m s^{-1}), and a single horizontal groundwater flux or "underflow" ($q_U=K_hS=10^{-5}$ m s^{-1}) (Table 1). Collectively, these 10 scenarios cover a realistic range of ambient stream and groundwater flows [e.g., *Schmidt et al.*, 2006; *Kennedy et al.*, 2009; *Englelhardt et al.*, 2011] and were specifically chosen so that we could incorporate into our study the results of a previously published computational fluid dynamics (CFD) study of hyporheic exchange across riffle-pool sequences [*Trauth et al.*, 2013, 2014].

3. Nitrate Evolution Along a HZT

3.1. Model of Subsurface Biogeochemistry

Our biokinetic model tracks the evolution of three chemical constituents (nitrate, oxygen, and ammonium) as a water parcel travels along a HZT. These three chemical constituents are produced and/or consumed by a coupled set of microbially mediated redox reactions, including aerobic respiration (AR), ammonification (AM), nitrification (NI), and denitrification (DN) [*National Environmental Research Institute*, 2004; *Cook et al.*, 2006; *Evrard et al.*, 2012]:

$$\mathrm{AR}: CH_2O+O_2 \rightarrow CO_2+H_2O \tag{3a}$$

$$\mathrm{DN}: CH_2O+0.8\ NO_3^- +0.8\ H^+ \rightarrow CO_2+0.4\ N_2+1.4\ H_2O \tag{3b}$$

$$\text{NI}: NH_4^+ + 2\ O_2 \rightarrow NO_3^- + 2H^+ + H_2O \tag{3c}$$

$$\text{AM}: \{NH_3\}_{OM} + H^+ \rightarrow NH_4^+ \tag{3d}$$

The temporary storage of N in microbial or plant biomass (assimilation) is not included, which is reasonable provided a steady state balance exists between N uptake by assimilation and N release by biomass decomposition and die-off (e.g., over weeks or longer timescales) [*Peterson et al.*, 2001]; however, up to a third of the N assimilated in plant tissues can be stored in stream sediments as refractory soil organic material [*Birgand et al.*, 2007]. Indeed, one of the goals of our study is to evaluate the importance of N assimilation—relative to the other components of the N cycle captured by equations (3a)–(3d)—by comparing our model predictions (which do not account for assimilation) with nitrate uptake velocities observed in reach-scale field experiments (section 6). Our biokinetic model also neglects anaerobic ammonium oxidation (Anammox) and dissimilatory nitrate reduction to ammonium (DNRA). Although important in some estuarine and marine settings, these alternative pathways for nitrate reduction are thought to be of secondary importance (relative to respiratory denitrification, equation (3b)) in rivers and streams [*Burgin and Hamilton*, 2007; *Hu et al.*, 2011; *Lansdown et al.*, 2016].

To translate the above redox reactions into predictions for the evolution of oxygen, nitrate, and ammonium concentration along a HZT, we invoke the following two assumptions: (1) water parcels behave like well-mixed batch reactors as they travel along a HZT (see the streamline segregation discussion in section 2.2); and (2) at any particular location in the sediment the concentration field and flow field are steady state (i.e., they do not change with time). Given these two assumptions, mass balance over a single water parcel yields the following set of coupled ordinary differential equations for the concentrations (units of mol m^{-3}) of molecular oxygen (C_{HZT-O_2}), nitrate ($C_{HZT-NO_3^-}$), and ammonium ($C_{HZT-NH_4^+}$) as function of travel time (τ) through a HZT:

$$\frac{dC_{HZT-O_2}}{d\tau} = -R_{AR} - 2R_{NI} \tag{4a}$$

$$\frac{dC_{HZT-NO_3^-}}{d\tau} = R_{NI} - R_{DN} \tag{4b}$$

$$\frac{dC_{HZT-NH_4^+}}{d\tau} = R_{AM} - R_{NI} \tag{4c}$$

Variables on the right hand side of these equations represent rates (units of mol m^{-3} s^{-1}) of aerobic respiration (R_{AR}), nitrification (R_{NI}), denitrification (R_{DN}), and ammonification (R_{AM}).

Following the procedure outlined in *Van Cappellenn and Wang* [1996] and *Berg et al.* [2003], we assume AR and DN follow saturation-type (Monod) rate expressions, NI is second-order in oxygen and ammonium concentrations, and AM is zero-order and proportional to the organic carbon mineralization rate (R_{min}, units mol m^{-3} s^{-1}) [see also *Cook et al.*, 2006; *Kessler et al.* 2013a, 2013b]. The organic carbon mineralization rate can be represented as the product of a first-order mineralization rate constant (k_{min}, units s^{-1}) and the interstitial concentration of dissolved organic carbon (C_{DOC}, units mol m^{-3}) [*Pett*, 1989; *Zarnetske et al.*, 2012]: $R_{min} = k_{min} C_{DOC}$. Thus, the potential effects of organic carbon limitation on denitrification [e.g., see *Taylor and Townsend*, 2010] are embodied in the value of R_{min}, which in our biokinetic model is assumed to be constant throughout the hyporheic zone:

$$R_{AR} = \frac{R_{min} C_{HZT-O_2}}{C_{HZT-O_2} + K_{O_2}^{sat}} \tag{5a}$$

$$R_{AM} = \frac{1}{\gamma_{CN}} R_{min} \tag{5b}$$

$$R_{NI} = k_{NI} C_{HZT-O_2} C_{HZT-NH_4^+} \tag{5c}$$

$$R_{DN} = \theta_{O_2}^{inh} \kappa \frac{R_{min} C_{HZT-NO_3^-}}{C_{HZT-NO_3^-} + K_{NO_3^-}^{sat}}; \theta_{O_2}^{inh} = \frac{K_{O_2}^{inh}}{C_{HZT-O_2} + K_{O_2}^{inh}} \tag{5d}$$

New variables appearing here include a fixed constant for the production of dissolved ammonium by the mineralization of organic carbon (γ_{CN}, unitless); a second-order nitrification rate constant (k_{NI}, units m^3 mol^{-1} s^{-1}); half-saturation constants for aerobic respiration ($K_{O_2}^{sat}$, units mol m^{-3}), denitrification ($K_{NO_3^-}^{sat}$, units mol m^{-3}), and oxygen inhibition of denitrification ($K_{O_2}^{inh}$, units mol m^{-3}); coefficient for the noncompetitive inhibition of

denitrification by molecular oxygen ($\theta_{O_2}^{inh}$); and a parameter (κ, unitless) that indicates the relative rate at which organic carbon is oxidized by aerobic respiration and respiratory denitrification.

Combining equations (4a) through (5d) and normalizing all variables to a dimensionless form, we arrive at the following set of coupled rate equations for the coevolution of molecular oxygen, nitrate, and ammonium with travel time through the hyporheic zone:

$$\frac{d\hat{C}_{HZT-O_2}}{d\hat{\tau}_R} = -\frac{\hat{C}_{HZT-O_2}}{\hat{C}_{HZT-O_2}/\hat{K}_{O_2}^{sat}+1} - 2\delta\hat{C}_{HZT-O_2}\hat{C}_{HZT-NH_4^+}, \hat{C}_{HZT-O_2}(\hat{\tau}_R=0)=1 \tag{6a}$$

$$\frac{d\hat{C}_{HZT-NO_3^-}}{d\hat{\tau}_R} = \delta\hat{C}_{HZT-O_2}\hat{C}_{HZT-NH_4^+} - \frac{\kappa\hat{K}_{O_2}^{inh}\hat{K}_{O_2}^{sat}\hat{C}_{HZT-NO_3^-}}{\left(\hat{C}_{HZT-O_2}+\hat{K}_{O_2}^{inh}\right)\left(\hat{C}_{HZT-NO_3^-}+\hat{K}_{NO_3^-}^{sat}\right)}, \tag{6b}$$

$$\hat{C}_{HZT-NO_3^-}(\hat{\tau}_R=0)=\beta$$

$$\frac{d\hat{C}_{HZT-NH_4^+}}{d\hat{\tau}_R} = \frac{1}{\gamma_{CN}}\hat{K}_{O_2}^{sat} - \delta\hat{C}_{HZT-O_2}\hat{C}_{HZT-NH_4^+}, \hat{C}_{HZT-NH_4^+}(\hat{\tau}_R=0)=\alpha \tag{6c}$$

In these equations, all variables with units of concentration have been normalized by the concentration of molecular oxygen in the stream: $\hat{C}_{HZT-O_2}=C_{HZT-O_2}/C_{S-O_2}$, $\hat{C}_{HZT-NO_3^-}=C_{HZT-NO_3^-}/C_{S-O_2}$, $\hat{C}_{HZT-NH_4^+}=C_{HZT-NH_4^+}/C_{S-O_2}$, $\hat{K}_{O_2}^{sat}=K_{O_2}^{sat}/C_{S-O_2}$, $\hat{K}_{NO_3^-}^{sat}=K_{NO_3^-}^{sat}/C_{S-O_2}$, $\hat{K}_{O_2}^{inh}=K_{O_2}^{inh}/C_{S-O_2}$, $\alpha=C_{S-NH_4^+}(\hat{\tau}_R=0)/C_{S-O_2}$, and $\beta=C_{S-NO_3^-}(\hat{\tau}_R=0)/C_{S-O_2}$. The dimensionless parameters δ and $\hat{\tau}_R$ represent the relative rates of nitrification and respiration ($\delta=k_{NI}C_{S-O_2}\tau_R$) and normalized travel time along a HZT ($\hat{\tau}_R=\tau/\tau_R$). The variable $\tau_R=K_{O_2}^{sat}/R_{min}$ (units s) is the timescale for organic carbon mineralization.

The benefit of rewriting our model in dimensionless form is that, by doing so, we reduce the number of model parameters by the number of physical units [*Buckingham*, 1914]. Because our biokinetic model has two physical units (mass concentration and time), we reduced its dimensionality from ten parameters (C_{S-O_2}, $C_{S-NO_3^-}$, $C_{S-NH_4^+}$, R_{min}, $K_{NO_3^-}^{sat}$, $K_{O_2}^{sat}$, $K_{O_2}^{inh}$, k_{NI}, γ_{CN}, κ) to eight parameters (δ, $\hat{K}_{O_2}^{sat}$, $\hat{K}_{NO_3^-}^{sat}$, $\hat{K}_{O_2}^{inh}$, α, β, γ_{CN}, κ). Once these eight dimensionless parameters are specified, equations (6a) through (6c) are numerically solved to yield the interstitial nitrate concentration as a function of travel time along a HZT; (see equation (1b) and supporting information Code 1). Next we describe the process by which we chose three sets of parameter values to represent a spectrum of streams, from pristine to polluted.

3.2. Selection of Biokinetic Model Parameters

3.2.1. In-Stream Concentrations and Ecosystem Respiration

In-stream concentrations of oxygen, nitrate, ammonium, and organic carbon tend to covary across different streams (i.e., they are not statistically independent, see *Taylor and Townsend* [2010]), and this covariance should be accounted for if we are to select realistic model parameters. To this end, we performed a principal component analysis (PCA) of C_{S-O_2}, $C_{S-NO_3^-}$, $C_{S-NH_4^+}$, and ecosystem respiration (ER, units mol m^{-2} s^{-1}) values measured in 70 stream sites across the United States (including reference streams, urban impacted streams, and agriculture impacted streams) as part of the Second Lotic Intersite Nitrate Experiment (LINX II) [*Mulholland et al.*, 2008, 2009; *Beaulieu et al.*, 2011]. The PCA was performed on log-transformed, mean-centered, and scaled (z-scored) data (details in supporting information Text S1), with the goal of identifying the dominant patterns, or PC modes, for these four chemical parameters across all 70 sites. A resampling-based stopping rule [*Peres-Neto et al.*, 2005; *Rippy et al.*, 2017] was used to identify PC modes that explained more variance in stream biogeochemistry than expected by chance (significant at $p < 0.1$). A nonparametric bootstrap approach [*Babamoradi et al.*, 2013] was used to determine the statistical uncertainty about significant PC modes and their corresponding scores: i.e., the location of individual reference, agricultural, and urban streams relative to the first two PC modes.

PCA identified two marginally significant PC modes ($p < 0.1$) that together capture approximately 67% of the biogeochemical variability in the LINX II data set (Figure 2 and supporting information Figure S1). PC Mode 1 (our primary pattern, 38% variance explained) predominantly reflects the ambient in-stream concentration of ammonium (i.e., PC Mode 1 aligns with the loading vector for NH_4^+), and separates reference streams (typically low $C_{S-NH_4^+}$) from urban and agriculture-impacted streams (low to high $C_{S-NH_4^+}$). PC Mode 2 (our secondary pattern, 29% variance explained) primarily reflects ER (i.e., PC Mode 2 aligns with the

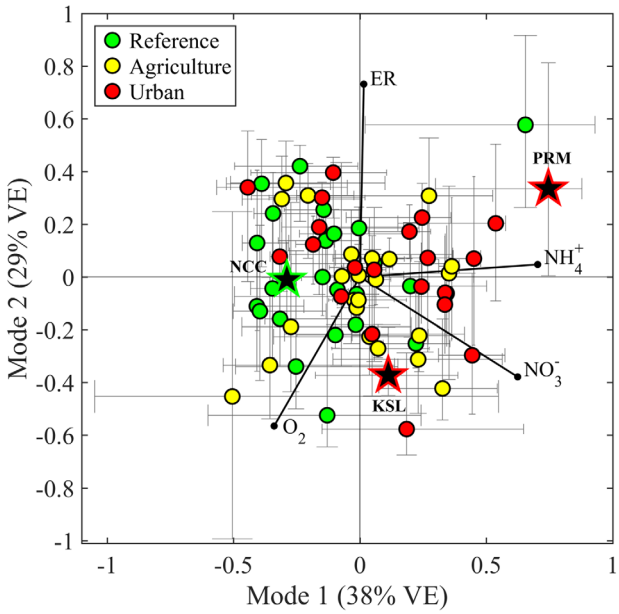

Figure 2. Principle Component Analysis (PCA) of ambient stream data measured at 70 stream sites included in the second Lotic Intersite Nitrogen Experiments (LINX II) study (data reproduced from *Mulholland et al.* [2008, 2009]; *Beaulieu et al.* [2011]). Sites include pristine or reference streams (green circles), agriculture impacted streams (yellow circles), and urban impacted streams (red circles); the error bars about these points are 95% resampling-based confidence intervals. The first two PCA modes explain 67% of the variance in log-transformed, z-scored measurements of ecosystem respiration (*ER*), and in-stream concentrations of ammonium (NH_4^+), nitrate (NO_3^-), and oxygen (O_2). Biogeochemical loading vectors for these four stream parameters are shown in black. Three sites were selected for biokinetic modeling (large colored stars), including Cunningham Creek in North Carolina (NCC), Rio Maymeyes Tributary in Puerto Rico (PRM), and Little Kitten Creek in Kansas (KSL).

loading vector for ER), but does not obviously separate the streams by type (i.e., reference, agriculture, or urban). The loading vector for molecular oxygen is associated with low $C_{S-NH_4^+}$ (negative values of Mode 1) and low ER (negative values of Mode 2). The loading vector for nitrate is associated with high ammonium concentrations (positive values of Mode 1) and low ER (negative values of Mode 2).

Overall, these PCA results are qualitatively consistent with the structure of our biokinetic model and previously published assessments of N-cycling in streams [e.g., *Birgand et al.*, 2007]. In particular, the following patterns are evident (Figure 2): (1) oxygen concentrations are low in streams with high ER, reflecting high organic carbon mineralization rates (large R_{min}) and high rates of aerobic respiration (large R_{AR}) (see equation (5a)); (2) nitrate concentrations are low in streams with high ER, reflecting high organic carbon mineralization rates (large R_{min}) and high denitrification rates (large R_{DN}) (see equation (5d)); and (3) ammonium concentrations are low in streams with high molecular oxygen concentrations, reflecting high rates of nitrification (large R_{NI}) (see equation (5c)). Intriguingly, the loading vector for nitrate is located midway between the oxygen and ammonium loading vectors, perhaps reflecting the importance of nitrification (which requires both oxygen and ammonium, see equation (5c)) in nitrate generation.

Based on the results presented in Figure 2, we selected three stream sites that collectively capture a diversity of biogeochemical settings (see colored stars): (1) Cunningham Creek in North Carolina (NCC) is characterized by low ammonium and nitrate concentrations, moderate molecular oxygen concentration, and moderate ER ($C_{S-O_2}=2.91\times10^{-1}$mol m^{-3}, $C_{S-NH_4^+}=2.14\times10^{-4}$ mol m^{-3}, $C_{S-NO_3^-}=7.14\times10^{-4}$ mol m^{-3}, ER$=1.88\times10^{-6}$ mol m^{-2} s^{-1}; (2) Rio Mameyes Tributary in Puerto Rico (PRM) is characterized by high ammonium, moderate nitrate, and low molecular oxygen concentrations, together with high ER ($C_{S-O_2}=1.34\times10^{-1}$ mol m^{-3}, $C_{S-NH_4^+}=1.57\times10^{-1}$ mol m^{-3}, $C_{S-NO_3^-}=1.24\times10^{-2}$ mol m^{-3}, ER$=2.68\times10^{-6}$ mol m^{-2} s^{-1}); and (3) Little Kitten Creek in Kansas (KSL) is characterized by moderate ammonium and nitrate concentrations, high oxygen concentration, and low ER ($C_{S-O_2}=2.60\times10^{-1}$ mol m^{-3}, $C_{S-NH_4^+}=1.71\times10^{-3}$ mol m^{-3}, $C_{S-NO_3^-}=1.20\times10^{-2}$ mol m^{-3}, ER$=3.26\times10^{-7}$ mol m^{-2} s^{-1}). While several LINX II sites had higher nitrate concentrations than KSL (i.e., plotted closer to the end of the NO_3^- loading vector), these were not selected for further study because: (1) nitrate uptake velocities were not measured or (2) sediment characteristics differed substantially from NCC and PRM (A. Marzadri, personal communication, 2017). Organic carbon mineralization rates at these three sites were calculated by dividing reported ER values by an order-of-magnitude estimate of the streambed depth over which mineralization occurs (~10 cm): $R_{min}=\mathrm{ER}/d$ where $d=0.1$ m. Accordingly, we adopted the following mineralization rates for NCC, PRM, and KSL, respectively: $R_{min}=1.88\times10^{-5}$ mol m^{-3} s^{-1}, $R_{min}=2.68\times10^{-5}$ mol m^{-3} s^{-1}, and $R_{min}=3.26\times10^{-6}$ mol m^{-3} s^{-1} (Table 2).

3.2.2. Half-Saturation Constants

Garcia-Ruiz et al. [1998] measured half-saturation constants for denitrification ($K^{sat}_{NO_3^-}$) in intact sediment cores collected from five sites along the Swale-Ouse river system in northeastern England, including one from a

Table 2. In-Stream and Hyporheic Zone "Chemistry" for Three Sites Selected From LINX II Data Set[a]

	NCC	PRM	KSL
Dimensional parameters (units)			
C_{S-O_2} (mol m^{-3})	2.91E-01	1.34E-01	2.60E-01
$C_{S-NH_4^+}$ (mol m^{-3})	2.14E-04	1.57E-01	1.71E-03
$C_{S-NO_3^-}$ (mol m^{-3})	7.14E-04	1.24E-02	1.20E-02
$K_{O_2}^{inh}$ (mol m^{-3})	3.00E-03	3.00E-03	3.00E-03
$K_{NO_3^-}^{sat}$ (mol m^{-3})	1.30E-02	9.00E-02	9.00E-02
$K_{O_2}^{sat}$(mol m^{-3})	6.00E-03	6.00E-03	6.00E-03
k_{NI} (m^3 mol^{-1} s^{-1})	4.00E-04	4.00E-04	4.00E-04
R_{min} (mol m^{-3} s^{-1})	1.88E-05	2.68E-05	3.26E-06
$\tau_R \equiv K_{O_2}^{sat}/R_{min}$ (s)	319	224	1840
Nondimensional parameters (unitless)			
$\delta \equiv \tau_R k_{NI} C_{S-O_2}$	3.72E-02	1.20E-02	1.91E-01
$\hat{K}_{O_2}^{sat} \equiv K_{O_2}^{sat}/C_{S-O_2}$	2.06E-02	4.48E-02	2.31E-02
$\hat{K}_{NO_3^-}^{sat} \equiv K_{NO_3^-}^{sat}/C_{S-O_2}$	4.46E-02	6.72E-01	3.47E-01
$\hat{K}_{O_2}^{inh} \equiv K_{O_2}^{inh}/C_{S-O_2}$	1.03E-02	2.24E-02	1.16E-02
$\alpha \equiv C_{S-NH_4^+}/C_{S-O_2}$	7.35E-04	1.17E+00	6.60E-03
$\beta \equiv C_{S-NO_3^-}/C_{S-O_2}$	2.45E-03	9.25E-02	4.62E-02
$\kappa \cong v_{f,Dw}(C_{S-NO_3^-}+K_{NO_3^-}^{sat})/ER$	0.11	0.36	0.38
γ_{CN}	14	14	14

[a]Cunningham Creek in North Carolina (NCC), Rio Mameyes Tributary in Puerto Rico (PRM), and Little Kitten Creek in Kansas (KSL) (variables defined in Notation section).

highly polluted tributary. The half-saturation constants range from $K_{NO_3^-}^{sat} = 0.013$ mol m^{-3} at the headwater site to $K_{NO_3^-}^{sat} = 0.09$ mol m^{-3} at the downstream site; the most polluted site had a half-saturation constant of $K_{NO_3^-}^{sat} = 0.64$ mol m^{-3}. These authors noted that their measured half-saturation constants increased along the river continuum (i.e., as ambient stream nitrate concentration increased), consistent with the idea that denitrifying microorganisms in streambed sediments have reduced nitrate affinity (i.e., higher half-saturation constants) at sites with high ambient stream nitrate concentrations. The authors also noted that their experimental approach (measuring denitrification rates after adding a fixed concentration of nitrate to the water overlying an intact sediment core) tends to overestimate the half-saturation constant [*Garcia-Ruiz et al.*, 1998]. Alternatively, *Evrard et al.* [2012] conducted denitrification measurements in flow through reactors specifically designed to mimic advective flow through permeable sediments; their half-saturation constants ($K_{NO_3^-}^{sat} = 0.0015$–$0.0198$ mol m^{-3}) are generally lower than the values reported by Garcia-Ruiz et al. (0.013–0.09 mol m^{-3}, excluding the most polluted site). While the different ranges reported in these two studies could reflect methodological differences (static incubations with intact cores versus flow through experiments in sediment columns), the ambient nitrate concentrations were also quite different; indeed, the highest ambient nitrate concentration used in Evrard et al.'s study (0.00493 mol m^{-3}) is more than twofold lower than the nitrate concentrations measured at our PRM and KSL sites (0.0124 and 0.0120 mol m^{-3}, respectively). In the end, we adopted Garcia-Ruiz et al.'s highest half-saturation constant (excluding the most polluted site) for our two urban impacted stream sites ($K_{NO_3^-}^{sat,KSL} = K_{NO_3^-}^{sat,PRM} = 0.09$ mol m^{-3}) and Garcia-Ruiz et al.'s lowest half-saturation constant for our pristine site ($K_{NO_3^-}^{sat,NCC} = 0.013$ mol m^{-3}) (Table 2). A single set of half-saturation constants was adopted for aerobic respiration ($K_{O_2}^{sat} = 0.006$ mol m^{-3}) and noncompetitive oxygen inhibition of denitrification ($K_{O_2}^{inh} = 0.003$ mol m^{-3}) [*Sawyer*, 2015] (Table 2).

3.2.3. Ammonification, Denitrification, and Nitrification

Ammonification was taken as a fixed fraction ($\gamma_{CN} = 14$) of the organic carbon mineralization rate [*Kessler et al.*, 2013b]. The denitrification rate depends on R_{min}, $K_{NO_3^-}^{sat}$, $K_{O_2}^{inh}$ (discussed above), as well as the constant κ. Given the stoichiometry of AR and DN (see equations (3a) and (3b)), aerobic respiration should consume one mole of organic carbon for every mole of molecular oxygen reduced, while denitrification should consume $\kappa = 1/0.8 = 1.25$ moles of organic carbon for every mole of nitrate reduced. However, recent laboratory and field observations of respiratory denitrification in coastal marine sediments indicate that κ is 25 times smaller ($\kappa = 0.05$) than the stoichiometric value ($\kappa = 1.25$) [*Evrard et al.*, 2012; *Kessler et al.*, 2013a, 2013b], perhaps reflecting the dominance of benthic algal metabolism in these systems [*Bourke et al.*, 2017]. To determine where along this spectrum (from $\kappa = 0.05$ to 1.25) our stream sites fall, we estimated κ as follows. Assuming the sediment is well-mixed and oxygen inhibition of denitrification in the bulk sediment is minimal ($\theta_{O_2}^{inh} \approx 1$), equation (5d) can be rearranged as follows: $\kappa \approx (R_{DN}/R_{min})(C_{S-NO_3^-}+K_{NO_3^-}^{sat})/C_{S-NO_3^-}$. The ratio R_{DN}/R_{min} can be approximated from the ratio of the flux of stream nitrate into the streambed by denitrification (U_{DN}, units mol m^{-2} s^{-1}) and the ecosystem respiration rate: $R_{DN}/R_{min} \approx U_{DN}/ER$. This last equality follows by multiplying the top and bottom of the ratio R_{DN}/R_{min} by the sediment depth d over which denitrification occurs, and recognizing that $U_{DN} \approx R_{DN}d$ and $ER \approx R_{min}d$ (see earlier discussion of estimating

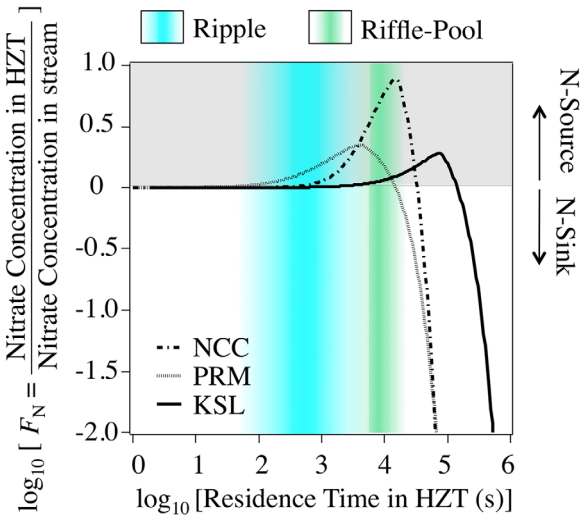

Figure 3. Fraction of stream nitrate remaining (F_N) as a function of travel time through a HZT, as predicted by our biokinetic model (equations (6a) through (6c)). Different curves correspond to three LINX II stream sites: NCC, PRM, and KSL (see caption for Figure 2 for details). The vertical bands of color indicate the distribution of residence times for fluvial ripples (turquoise) and riffle-pool sequences (green).

R_{min} from ER). Combining these results, we obtain the formula: $\kappa \approx v_{f,Dw}(C_{S-NO_3^-} + K^{sat}_{NO_3^-})/ER$ where $v_{f,Dw}$ (units m s^{-1}) is the uptake velocity of stream nitrate by direct denitrification: $v_{f,Dw} \equiv U_{DN}/C_{S-NO_3^-}$. From $^{15}NO_3^-$-seeding experiments, *Mulholland et al.* [2008] estimated values for $v_{f,Dw}$ for most of the LINX II sites (note that $v_{f,Dw}$ is notated as v_{fden} in their paper). Thus, all of the variables needed to estimate κ for our three sites were either known ($v_{f,Dw}$, $C_{S-NO_3^-}$, ER) or previously estimated from the literature (see last section, $K^{sat}_{NO_3^-}$). After substituting these values into our formula, we obtain: $\kappa = 0.11$, 0.38, and 0.36 for NCC, KSL, and PRM, respectively (Table 2); these values were adopted in the modeling studies presented below. Intriguingly, these estimates of κ are skewed toward the previous estimate for permeable marine sediments ($\kappa = 0.05$), perhaps signalling the importance of benthic algal metabolism in both freshwater streams and coastal marine systems. Finally, the second-order nitrification rate constant was estimated from the nitrification parameters reported by *Zarnetske et al.* [2012] for Drift Creek, Oregon (USA): $k_{NI} = 0.0004$ m^3 mol^{-1} s^{-1} (Table 2).

3.3. Biokinetic Model Predictions for the Evolution of Nitrate Along a HZT

Biokinetic model predictions for the evolution of NO_3^- with travel time through the hyporheic zone are presented in Figure 3. These results are presented in terms of the fraction $F_N(\tau)$ (introduced in section 2.1), which represents the fraction of nitrate remaining after a water parcel travels through a HZT of residence time τ (see equation (2b)). For very short travel times ($\tau < 100$ s), there is insufficient time for biogeochemical reactions to occur and the interstitial nitrate concentration is unchanged (i.e. $F_N = 1$). For larger travel times, the nitrate concentration evolves in a similar manner across the three sites, first increasing above ambient stream concentrations ($F_N > 1$, due to the net production of nitrate by nitrification) and then declining after the oxic-anoxic transition ($F_N < 1$, as microbial metabolism switches from aerobic respiration to respiratory denitrification). The primary source of new nitrate at KSL is nitrification of ammonium downwelled into the hyporheic zone from the stream. The primary source of new nitrate at NCC is nitrification of ammonium produced within the hyporheic zone by ammonification (i.e., respiration of sediment organic material). The new nitrate at PRM is generated by nitrification of both stream-borne ammonium and ammonium generated in situ by ammonification. The residence time at which F_N drops below unity decreases in order: KSL > NCC > PRM. This sequence precisely matches the respiration timescales for these three environments ($\tau_R = 1840$, 319, 224 s, respectively; see Table 2).

4. Hyporheic Exchange Flux and Ambient Groundwater

Hyporheic exchange flux (q_H) refers to the volume of water per unit streambed area per time that circulates between the hyporheic zone and the stream; it excludes vertical ambient groundwater flux (q_V) that moves in only one direction, either from the stream to the sediment under losing conditions or vice versa under gaining conditions. The hyporheic exchange flux is particularly important in the PASS model, because it is the only mechanism by which mass is transported across the sediment-water interface. Also, as noted in section 2.1, in the limit where all nitrate is removed by denitrification (i.e., the MTL, $\bar{C}_{HZT-NO_3^-} = 0$), the magnitude of the nitrate uptake velocity is determined solely by the hyporheic exchange flux: $v_{f,MTL} = -q_H$. Below we examine how ambient groundwater conditions affect the value of q_H across two bed form scales; namely riffle-pool sequences and fluvial ripples.

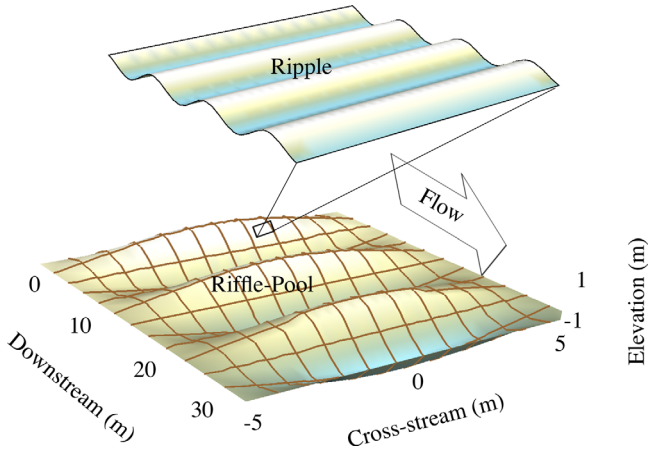

Figure 4. Idealized bed form topography assumed for submerged riffle-pool sequences (bottom surface) and fluvial ripples (inset). It should be noted that, depending on sediment grain size and stream velocity, fluvial ripples and riffle-pool sequences may not cooccur in natural streams [*Leeder*, 2012].

4.1. Riffle-Pool Sequences

4.1.1. Trauth et al.'s CFD Analysis

Trauth et al. [2013, 2014] performed CFD simulations of steady state turbulent stream flow over an idealized three-dimensional and fully submerged riffle-pool sequence with a bed slope of $S = 2\%$ and a stream width of $W = 10$ m (streambed topography is reproduced in Figure 4, lower surface). The period and amplitude of the riffle-pool features were 10 m and 0.5 m, respectively, while the average depth and velocity of the stream were 0.7 m and 1.15 m s^{-1} (for the low discharge scenario, L-Q) and 1 m and 1.95 m s^{-1} (for the high discharge scenario, H-Q) (Table 1). These CFD simulations yielded pressure distributions over the sediment-water interface, from which Trauth et al. calculated from Darcy's Law hyporheic exchange flow fields subject to an imposed upward ($q_V > 0$, gaining stream) or downward ($q_V < 0$, losing stream) vertical groundwater flux and constant underflow ($q_U = K_h S = 10^{-5}$ m s^{-1}).

4.1.2. Hyporheic Exchange Flux across Riffle-Pool Sequences

Trauth et al.'s simulations of hyporheic exchange flux (q_H, units m s^{-1}) for the 10 flow scenarios are reproduced in Figure 5 (dark green and dark orange bars). All else being equal, the hyporheic exchange flux across riffle-pool sequences: (1) is approximately 25% larger for simulations conducted at higher discharge (compare dark orange and dark green bars), and (2) declines sharply with vertical ambient groundwater flux (see reduction in dark orange and dark green bars as the magnitude of q_v increases). The reduction in q_H is similar (although not identical) for gaining ($q_V > 0$) and losing ($q_V < 0$) conditions. The slight asymmetry arises because, for a three-dimensional streambed, hyporheic flow paths are suppressed by groundwater flux in different parts of the sediment-water interface under gaining and losing conditions [*Trauth et al.*, 2013, 2014].

4.2. Fluvial Ripples

4.2.1. Boano et al.'s Advective Pumping Model

Elliott and Brooks derived an analytical solution for hyporheic exchange across fluvial ripples [*Elliott and Brooks*, 1997a, 1997b]. Their so-called advective pumping model, which assumes that hyporheic exchange is driven by a sinusoidal pressure variation over a flat sediment-water interface, was modified by *Boano et al.* [2008, 2009] to account for vertical (q_V) and horizontal (q_U) ambient groundwater fluxes (see supporting information Text S2 for details). Boano et al.'s formula for the hyporheic exchange flux is given as follows:

$$q_H = q_{H,0}\sqrt{1-\left(q_V/\pi q_{H,0}\right)^2} + \left(|q_V|/\pi\right)\sin^{-1}\left(|q_V|/\pi q_{H,0}\right) - \left(|q_V|/2\right) \tag{7a}$$

$$q_{H,0} = 2K_h h_0/\lambda \tag{7b}$$

$$h_0 = a\frac{U^2}{2g}\left(\frac{H}{0.34d_s}\right)^m \tag{7c}$$

$$\tau_T = \lambda\theta/\left(2\pi^2 q_{H,0}\right) \tag{7d}$$

New variables appearing here include: a characteristic hyporheic exchange flux ($q_{H,0}$); the amplitude of the dynamic pressure head perturbation over the ripple (h_0, units m); the ripple height (H, units of m) and wavelength (λ, units of m); stream depth (d_s, units m) and mean velocity (U, units m s^{-1}); the gravitational constant ($g = 9.81$ m s^{-2}); two empirical constants (a, m, both unitless); and a characteristic transport timescale for hyporheic exchange (τ_T, units s). Equation (7c) is based on flume measurements of the dynamic pressure head over the surface of triangular dunes submerged in a turbulent stream [*Fehlman*, 1985]. While Boano

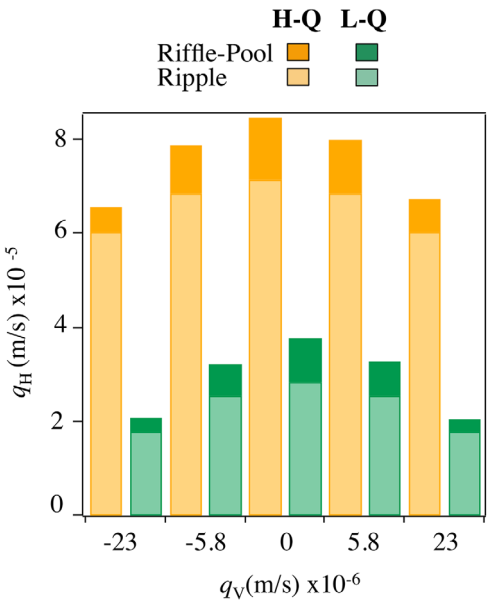

Figure 5. Hyporheic exchange flux (q_H) predicted for riffle-pool sequences (dark shades) and fluvial ripples (light shades) in the presence of ambient vertical groundwater flux ($q_V = 0$, $q_V > 0$, and $q_V < 0$ denote neutral, gaining, and losing conditions, respectively), a constant groundwater underflow ($q_U = 10^{-5}$ m s^{-1}), and two stream discharges ($Q = 7.4$ m^3 s^{-1} (L-Q, green bars) and 17.47 m^3 s^{-1} (H-Q, orange bars)). Hyporheic exchange fluxes reported for the riffle-pool sequences are reproduced from *Trauth et al.* [2013]; hyporheic exchange fluxes reported for fluvial ripples were calculated from equations (7a) through (7c) in this paper.

et al.'s solution assumes that the streambed is infinitely deep, analogous solutions have been derived for a sediment bed of finite depth with [*Marzadri et al.*, 2015] or without [*Packman et al.*, 2000] vertical ambient groundwater flow.

The hyporheic exchange flux across fluvial ripples was calculated from equation (7a) for the 10 ambient flow scenarios described earlier. To this end we adopted ripple dimensions ($H = 0.02$ m and $\lambda = 0.15$ m) and empirical constants ($a = 0.16$ and $m = 3/8$) reported in an experimental flume study by *Fox et al.* [2014] (see inset, Figure 4). All other variables were chosen to be consistent with the Trauth et al.'s CFD simulations described earlier (see section 4.1.1), including stream depth ($d_s = 1$ and 0.7 m for H-Q and L-Q, respectively), average stream velocity ($U = 1.95$ and 1.15 units m s^{-1} for H-Q and L-Q, respectively), stream slope ($S = 2\%$), porosity ($\theta = 0.3$), ambient groundwater flow ($q_U = 10^{-5}$ m s^{-1} and $q_v = 0$, $\pm 5.8\times10^{-6}$, $\pm 23\times10^{-6}$ m s^{-1}), and streambed hydraulic conductivity ($K_h = 5\times10^{-4}$m s^{-1}) (Table 1).

4.2.2. Hyporheic Exchange Flux Across Fluvial Ripples

All else being equal and despite their much smaller size, fluvial ripples generate 3–11 times more hyporheic exchange flux than riffle-pool sequences (Figure 5, compare light and dark-colored bars). Compared to riffle-pool sequences, the hyporheic exchange flux across ripples is more sensitive to stream discharge (compare light orange and light green bars) and less sensitive to vertical ambient groundwater flow (increasing magnitude of q_v). Because Boano et al.'s model assumes that the sediment-water interface is flat, the hyporheic exchange flux calculated from equation (7a) declines symmetrically under gaining or losing conditions (see supporting information Text S3 for a discussion of the symmetry properties of Boano et al.'s model).

5. Residence Time Distributions

The PASS model also requires specification of the RTD of water parcels undergoing hyporheic exchange, expressed as a probability density function (PDF) ($E(\tau)$, units s^{-1}, see equation (1b)). As mentioned earlier, $E(\tau)d\tau$ represents the fraction of water circulating through the hyporheic zone with a residence time within $d\tau$ of τ. Likewise, we can define a cumulative distribution function (CDF) form of the RTD (F_{RTD}, unitless), which represents the fraction of water circulating through the hyporheic zone with a residence time τ or younger. The PDF and CDF forms of the RTD are related in the usual way: $E(\tau) = dF_{RTD}/d\tau$.

As will be seen shortly, the residence time of water parcels undergoing hyporheic exchange varies over many orders of magnitude. The question then arises: what is the best way to represent such probability distributions graphically? An analogous situation arises for environmental particle size distributions (for example aerosols), and such distributions are routinely displayed by dividing the PDF into evenly spaced logarithmic increments of particle diameter [*Friedlander*, 2000]. Applied to our RTDs, this approach requires the specification of a new PDF (designated here as $E(\log_{10}\tau)$) that divides the fraction of water circulating through the hyporheic zone into equally spaced logarithmic intervals of residence time:

$$E(\log_{10}\tau) = \frac{dF_{RTD}}{d\log_{10}\tau} = 2.303\tau E(\tau) \tag{8}$$

The second equal sign in equation (8) follows from evaluating the derivative in the denominator, and then substituting the definition of $E(\tau)$. There are several advantages associated with representing the hyporheic

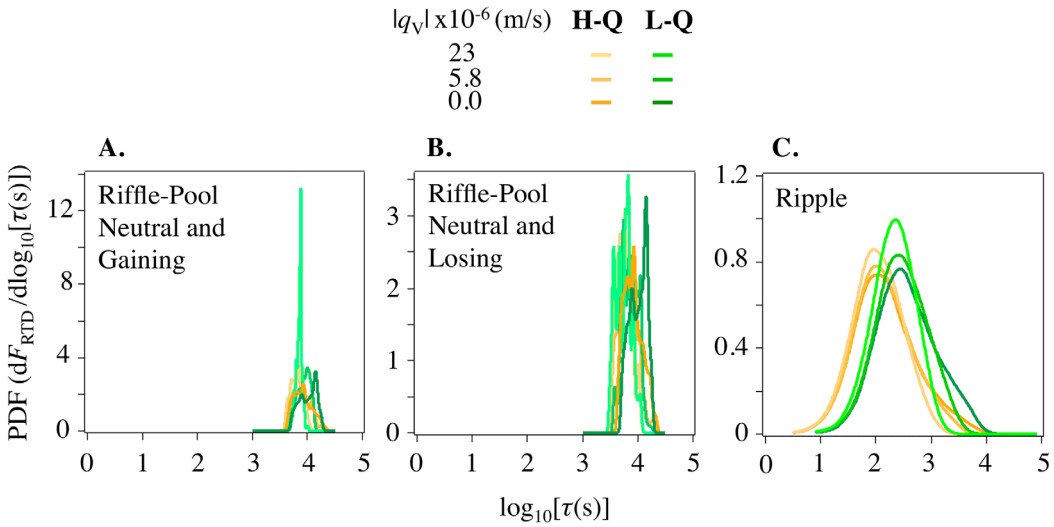

Figure 6. Simulated residence time distributions (RTDs) for: (a) riffle-pool sequences under neutral and gaining conditions; (b) riffle-pool sequences under neutral and losing conditions; and (c) fluvial ripples under neutral, gaining, and losing conditions. The curves are colored to represent the ten ambient flow scenarios described in the text. RTDs in Figures 6a and 6b are reproduced from *Trauth et al*. [2013]; RTDs in Figure 6c were calculated from the formula derived in this paper (see equations (9a) through (9c)).

zone RTDs as plots of $E(\log_{10}\tau)$ against $\log_{10}\tau$: (1) the RTD can be evaluated over many log-cycle changes in residence time τ; (2) the area under such curves is always unity, which allows for the direct comparison of RTDs associated with different scales of hyporheic exchange and different ambient flow conditions; and (3) the physical interpretation of such plots is straightforward, because the height of the curve at any point represents the probability density associated with a particular logarithmic interval of residence time. Below we adopt this approach to investigate the effects of changing ambient groundwater on the RTDs for riffle-pool sequences and fluvial ripples.

5.1. RTD of Water Circulating Through Riffle-Pool Sequences

Using numerical particle-tracking techniques, *Trauth et al*. generated RTDs for each of the ten CFD simulations described earlier (see sections 4.1.1 and 4.1.2). These RTDs, which are reproduced in Figures 6a and 6b, have a primary mode at around 3 h ($\tau \approx 10^4$s) and are confined to a relatively narrow range of log-transformed residence times ($\tau \approx 10^{3.6}$ to $10^{4.3}$s). The RTDs shift leftward (toward shorter residence times) when vertical groundwater flux is "turned on" (i.e., when the groundwater flux is changed from neutral to losing or gaining). This pattern is particularly apparent at low discharge (see dark to light green curves in Figures 6a and 6b).

5.2. RTD of Water Circulating Through Fluvial Ripples

5.2.1. Derivation of a New Analytical Solution for the RTD of Fluvial Ripples

Elliott and Brooks derived a formula for the RTD of water parcels undergoing hyporheic exchange; however, their formula does not account for ambient groundwater flow [*Elliott and Brooks*, 1997a, 1997b]. Here we derive a new RTD formula that is based on Boano et al.'s model of hyporheic exchange (see section 4.2.1) and explicitly accounts for ambient groundwater flow of arbitrary orientation and magnitude.

Before we present the new RTD formula, however, it is important to understand how ambient groundwater flow affects the hyporheic exchange flow field. To illustrate, in Figure 7 we present an example of the subsurface flow field predicted by Boano et al.'s model for one of 10 ambient flow conditions; namely low stream discharge (L-Q) and vertical and horizontal groundwater flow of $q_V = 2.3\times10^{-5}$ m s^{-1} and $q_U = 10^{-5}$ m s^{-1}, respectively. Noteworthy features of this hyporheic exchange flow field include: (1) when groundwater flow cannot be neglected (i.e., $q_V \neq 0$ and/or $q_U \neq 0$) hyporheic exchange occurs within a defined region of the sediment bed referred to as the interfacial exchange zone (IEZ, see the portion of the sediment bed contained within the thick black curve in the figure) [*Cardenas and Wilson*, 2007a, 2007b; *Cardenas*, 2008; *Cardenas et al*., 2008]; (2) within the IEZ, there are two flow cells, one located on the upstream side of the IEZ, and another located on the downstream side of the IEZ (denoted "upstream cell" and "downstream

cell" in the figure); (3) the upstream and downstream flow cells are symmetrical when there is no underflow (i.e., when $q_U=0$), and asymmetrical otherwise (the upstream and downstream cells in Figure 7 are asymmetrical because $q_U \neq 0$ in this case); and (4) because the upstream and downstream circulation cells are not, in general, symmetrical, the overall RTD (F_{RTD}) has contributions from both the upstream (F_1) and downstream (F_2) circulation cells (see supporting information Text S4 for derivation):

$$F_{RTD}(\bar{\tau})=F_1(\bar{\tau})+F_2(\bar{\tau}) \tag{9a}$$

$$F_1(\bar{\tau})=\frac{|\bar{q}_V|\left(\bar{x}_0^{up-cell}(\bar{\tau})-\sin^{-1}|\bar{q}_V|\right)-\sqrt{1-|\bar{q}_V|^2}+\cos\left[\bar{x}_0^{up-cell}(\bar{\tau})\right]}{2\left(|\bar{q}_V|(\pi/2-\sin^{-1}|\bar{q}_V|)-\sqrt{1-|\bar{q}_V|^2}\right)} \tag{9b}$$

$$F_2(\bar{\tau})=\frac{-|\bar{q}_V|\left(\bar{x}_0^{down-cell}(\bar{\tau})+\sin^{-1}|\bar{q}_V|-\pi\right)-\sqrt{1-|\bar{q}_V|^2}-\cos\left[\bar{x}_0^{down-cell}(\bar{\tau})\right]}{2\left(|\bar{q}_V|(\pi/2-\sin^{-1}|\bar{q}_V|)-\sqrt{1-|\bar{q}_V|^2}\right)} \tag{9c}$$

New variables appearing here include a normalized form of the vertical groundwater flux ($\bar{q}_V=q_V/(\pi q_{H,0})$) and the location along the sediment-water interface where water first enters the hyporheic zone in the upstream ($\bar{x}_0^{up-cell}=2\pi x_0^{up-cell}/\lambda$) or downstream ($\bar{x}_0^{down-cell}=2\pi x_0^{down-cell}/\lambda$) flow cells.

As currently written, our RTD formula (equations (9a) through (9c)) is expressed as a function of the streamline starting positions $\bar{x}_0^{up-cell}$ and $\bar{x}_0^{down-cell}$; these two variables are, in turn, a function of residence time τ. Indeed, as illustrated for two streamlines in Figure 7, each HZT passing through the upstream or downstream flow cell has a unique: (1) starting position (where water from the stream first enters the HZT, $\bar{x}_0=2\pi x_0/\lambda$); (2) final position (where water exits the HZT and returns to the stream, $\bar{x}_f=2\pi x_f/\lambda$); and (3) travel time ($\tau$) between these two locations. For any starting position ($\bar{x}_0$) in the upstream or downstream flow cell, the corresponding value of τ can be calculated by numerically solving the following set of coupled ordinary differential equations for the trajectory of a water parcel through the hyporheic zone, and recording the residence time τ at which the water parcel crosses the sediment-water interface and returns to the stream:

$$\bar{x}'(\bar{\tau})=-\cos\bar{x}(\bar{\tau})e^{\bar{y}(\bar{\tau})}+\bar{q}_U \tag{10a}$$

$$\bar{y}'(\bar{\tau})=-\sin\bar{x}(\bar{\tau})e^{\bar{y}(\bar{\tau})}+\bar{q}_V \tag{10b}$$

$$\bar{x}(0)=\bar{x}_0,\bar{y}(0)=0 \tag{10c}$$

New variables appearing here include normalized forms of the horizontal ($\bar{x}=2\pi x/\lambda$) and vertical ($\bar{y}=2\pi y/\lambda$) coordinates, horizontal groundwater flux ($\bar{q}_U=q_U/(\pi q_{H,0})$), and travel time through the hyporheic zone ($\bar{\tau}=\tau/\tau_T=2\pi^2 q_{H,0}\tau/(\lambda\theta)$, where τ_T (units, s) is a characteristic travel time). A procedure for numerically implementing our RTD solution is described in supporting information (see Text S5 and Code 2), along with a comparison of RTDs generated with our formula and new and previously published particle tracking results (supporting information Text S6).

5.2.2. The RTD Results

When our new formula (equations (9) and (10)) is applied to the ten ambient flow conditions described earlier, the resulting RTDs span a very broad range of residence times, from 10 to 10,000 s (Figure 6c). Each of these RTDs has a single mode (centered around $10^{2.4}$ and $10^{1.9}$ s for the L-Q and H-Q scenarios, respectively); interestingly, the RTDs display only a single mode, despite the fact that hyporheic exchange in this case involves circulation through separate (upstream and downstream) circulation cells (see Figure 7 and discussion thereof). Increasing stream discharge (from L-Q to H-Q) shifts the mode to shorter residence times (compare green and orange RTDs, Figure 6c). Increasing the ambient groundwater flow, on the other hand, has relatively little effect on either the shape or location of the RTDs, other than to slightly truncate the upper tail and increase the probability density associated with the mode. It should be noted that, for the largest vertical groundwater flux tested ($|q_V|=23\times10^{-6}$m s^{-1}), the ratio $|q_V|/q_H$ ranged from 0.38 to 1.3. Thus, our observation that increasing vertical groundwater flux has little impact on the RTD cannot be dismissed as an artifact of choosing vertical groundwater fluxes that are much smaller than the hyporheic exchange flux. Indeed, *Fox et al.* [2016] reached a similar conclusion, based on flume measurements of

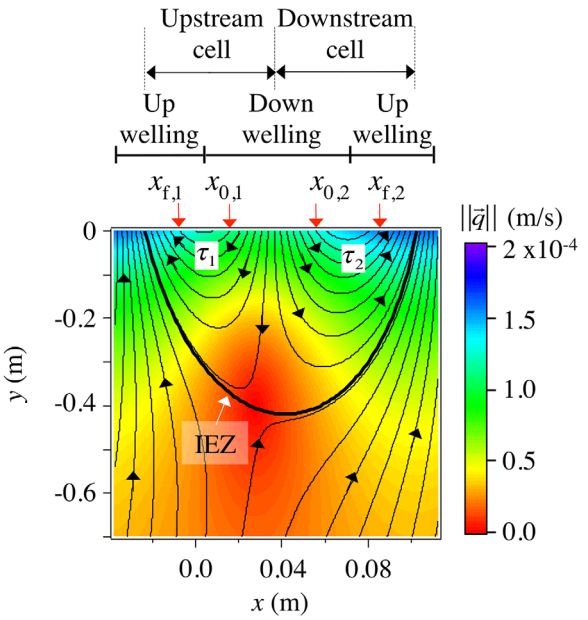

Figure 7. Hyporheic exchange in the presence of ambient groundwater flow, as predicted by *Boano et al.*'s model [2008, 2009]. In this example, streamflow above the sediment-water interface ($y > 0$) is from left to right, the wavelength of the fluvial ripple is 0.15 m, the stream discharge is 7.4 m^3 s^{-1}, and the vertical and underflow groundwater fluxes are 2.3$\times$ 10^{-5} and 10^{-5}m s^{-1}, respectively. Negative y values represent depth into the sediment bed, x is distance parallel to sediment-water interface (which is assumed to be flat), and color represents the modulus of the Darcy flux. Stream water is pumped into the sediment in high-pressure regions ("downwelling") and back into the stream in low-pressure regions ("upwelling"). Hyporheic exchange is confined to an Interfacial Exchange Zone (IEZ, bold black curve) that includes upstream and downstream flow cells. All streamlines (represented by the thin black curves) have a unique residence time (τ), starting point (x_0), and ending point (x_f); two streamlines have been labeled with subscripts "1" and "2" in the upstream and downstream flow cells, respectively. In this rendering, the volumetric flow rate per unit width between any two adjacent streamlines is the same and equal to $0.2\lambda q_{H,0}$ (see supporting information Text S3 for further details).

hyporheic exchange in the presence of an imposed vertical groundwater flux. These authors noted that the mean residence time of water undergoing hyporheic exchange varies only modestly when the groundwater flux is increased in either a gaining or losing configuration.

6. PASS Model Predictions for the Nitrate Uptake Velocity

We now have all of the information—evolution of the nitrate concentration with residence time, hyporheic exchange fluxes, and RTDs—required to calculate nitrate uptake velocities from the PASS model (see equations (1a) and (1b)). In the discussion below, we present results for three different forms of the nitrate uptake velocity: (1) total uptake defined as the flux of nitrate out of the sediment ($U_{NO_3^-}$, units mol m^{-2} s^{-1}) normalized by the in-stream concentration of nitrate ($v_f = U_{NO_3^-}/C_{S-NO_3^-}$, units of m s^{-1}); (2) direct denitrification of stream nitrate, defined as two times the flux of nitrogen gas generated by the denitrification of stream nitrate ($2U_{N_2,Dw}$, units mol m^{-2} s^{-1}) normalized by the in-stream concentration of nitrate ($v_{f,Dw} = 2U_{N_2,Dw}/C_{S-NO_3^-}$, units of m s^{-1}) (note that the factor of two is included here because, during denitrification, two molecules of nitrate are reduced for every molecule of N_2 generated); and (3) coupled nitrification-denitrification of ammonium downwelled from the stream or generated in situ by ammonification, defined as two times the flux of dinitrogen gas generated by the denitrification of new nitrate ($2U_{N_2,Dn}$, units mol m^{-2} s^{-1}) normalized by the in-stream concentration of nitrate ($v_{f,Dn} = 2U_{N_2,Dn}/C_{S-NO_3^-}$, units of m s^{-1}).

Together these three forms of the nitrate uptake velocity provide a complete accounting of the ways nitrate is generated and removed in the hyporheic zone, and are useful in different contexts. For example, the total nitrate uptake velocity (v_f) is of great practical interest, because the sign and magnitude of this quantity indicates whether, and to what extent, the sediments are a net source of nitrate (by net nitrification, $v_f > 0$) or a net sink of nitrate (by net denitrification, $v_f < 0$). On the other hand, field studies that quantify the rate at which stream nitrate is denitrified to N_2 (e.g., as v_{fden} values estimated from the LINX II $^{15}NO_3^-$ seeding studies [*Mulholland et al.*, 2008], see section 3.2) will be directly comparable to our model-predictions of $v_{f,Dw}$. Finally, studies of coupled nitrification-denitrification (e.g., using $^{15}NH_4^+$ seeding experiments as in *Peterson et al.* [2001], or the isotope pairing method of *Nielsen and Sloth* [1994]) will be directly comparable to our model-predictions of $v_{f,Dn}$. A Mathematica script for calculating the three forms of uptake velocity is presented in supporting information (Code 3). Our model-predictions for the three uptake velocities (v_f, $v_{f,Dw}$, $v_{f,Dn}$) are tabulated for all scenarios in the supporting information Table S2 and S3 and described below.

6.1. Effect of Stream Chemistry

Our model simulations predict that streambed sediments are a net source of nitrate at all three sites ($v_f > 0$, net nitrification), with v_f decreasing in order: NCC > PRM > KSL (Figure 8, compare vertical axes). At first glance, it is surprising that the pristine site (NCC) would have the largest v_f value. This can be explained by

the site's low nitrate concentration ($C_{S-NO_3^-} = 0.0007$ mol m^{-3}, see Table 2), which makes even a small nitrate flux manifest as a large positive nitrate uptake velocity (recall, $v_f \propto 1/C_{S-NO_3^-}$).

Uptake velocities for direct denitrification of stream nitrate ($v_{f,Dw}$, Figures 9a–9c) and coupled nitrification-denitrification ($v_{f,Dn}$, Figures 9d–9f) varies across the three sites, declining in order: PRM > NCC > KSL. Respiration time scales exhibit the opposite order (KSL ≫ NCC > PRM, see Table 2), which is expected given that denitrification occurs faster at sites with shorter respiration timescales.

Our prediction that streambed sediments are a net source of nitrate ($v_f > 0$, Figure 8) is contrary to the general observation that streambeds are a net sink of nitrate [*Birgand et al*., 2007], although there are notable exceptions [*Holmes et al*., 1994; *Ribot et al*., 2012]. There are at least two possible explanations for this discrepancy. First, as noted earlier, our model does not account for assimilation of nitrate by benthic autotrophic and heterotrophic organisms, and assimilation is known to dominate uptake velocities in many streams. For example, *Mulholland et al*. [2008] found that assimilation accounted for between 57 and 84% of the nitrate uptake observed in the LINX II $^{15}NO_3^-$-seeding studies, although some of the assimilated nitrate will be remineralized and released back to the stream over time scales of weeks to years [*Peterson et al*., 2001; *Mulholland et al*., 2000]. Second, our model may overestimate the generation of nitrate, either by overestimating in situ nitrification rates and/or overestimating the generation of ammonium by ammonification. In a multimethod study of N-cycling in the upper Mississippi River basin (USA), *Bohlke et al*. [2009] found that most of the nitrate being denitrified in streambed sediments was downwelled from the stream (direct denitrification of stream nitrate), and to a lesser extent supplied by in situ nitrification of ammonium (coupled nitrification-denitrification). These authors went on to note that coupled nitrification-denitrification is more common in estuarine or marine systems, which have "lower NO_3^- concentrations, higher sediment NH_4^+ concentrations, and steeper subbottom redox gradients." With the exception of the KSL site, our model predictions for $v_{f,Dn}$ (Figures 9d and 9e) are similar (PRM) or larger (NCC) in magnitude than model predictions for $v_{f,Dw}$ (Figures 9a and 9b). Thus, at PRM and NCC our model predicts that coupled nitrification-denitrification is a significant fraction of total denitrification, in violation of field observations for freshwater streams.

There are several reasons our model may overestimate nitrification rates. Our biokinetic model assumes that the organic carbon mineralization rate (R_{min}) is constant, whereas in reality R_{min} declines with travel time through the hyporheic zone [*Zarnetske et al*., 2015]. Our model also assumes that all ammonium produced by ammonification or downwelled from the stream is available for nitrification, when in reality a portion of the ammonium will sorb to stream sediments or undergo biological assimilation. Indeed, based on $^{15}NH_4^+$ stream seeding studies, *Peterson et al*. [2001] concluded that ammonium is removed primarily by assimilation and sorption to sediments, and "secondarily by nitrification." These model limitations can be

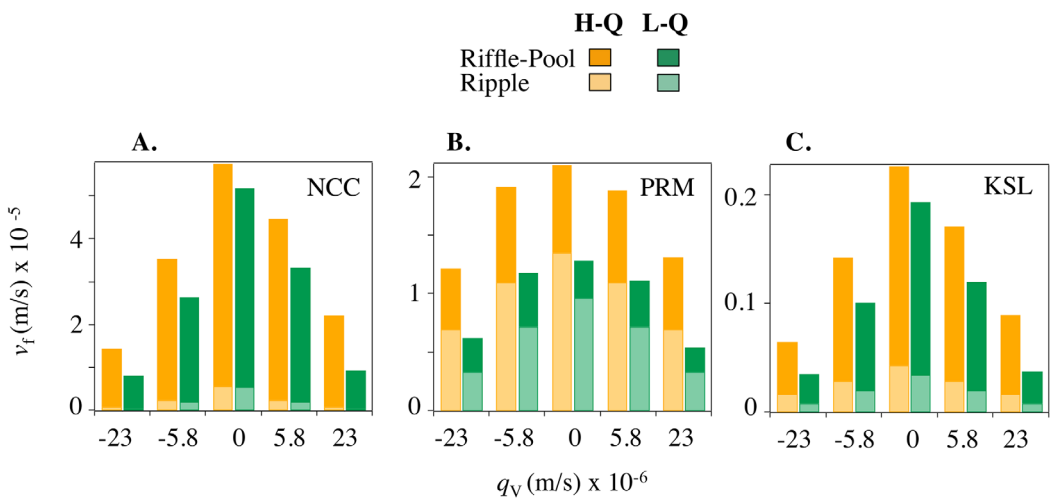

Figure 8. Model-predicted response of the total nitrate uptake velocity (v_f) to stream discharge (orange and green bars), bed form scale (light and dark shades), vertical ambient groundwater flux (horizontal axes), and biogeochemistry at the three LINX II stream sites: (a) NCC, (b) PRM, and (c) KSL (compare with Figure 5).

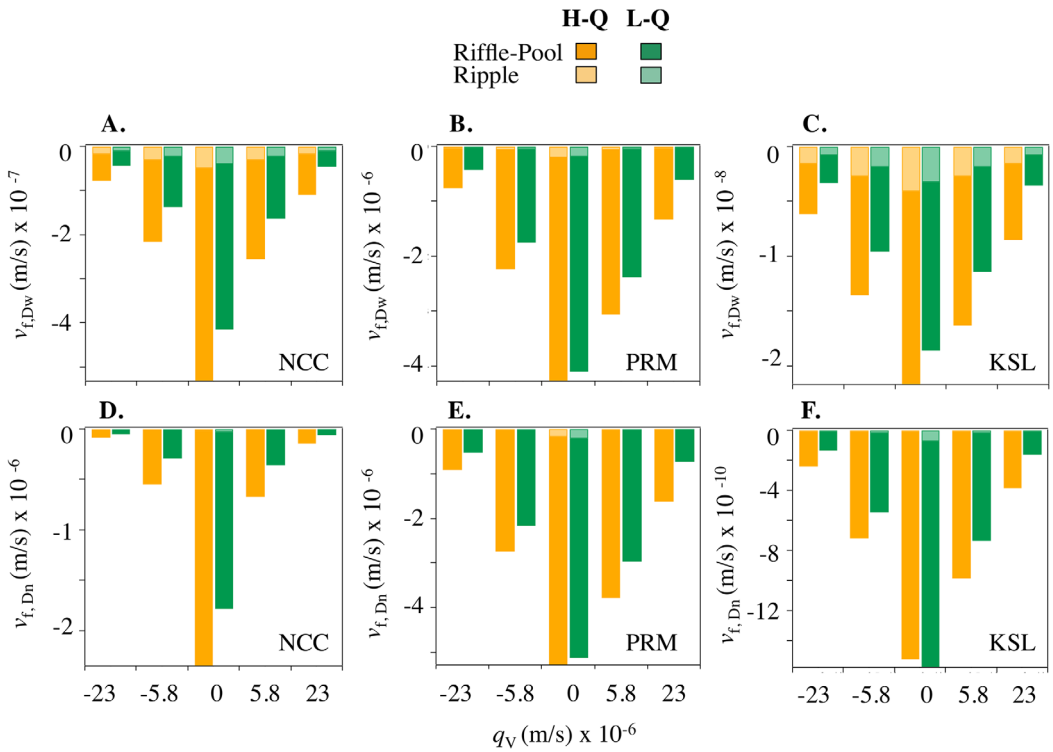

Figure 9. (a–c) Model-predicted response of the uptake velocities for direct denitrification of stream nitrate ($v_{f,Dw}$) and (d–f) coupled nitrification-denitrification ($v_{f,Dn}$) to stream discharge (orange and green bars), bed form scale (light and dark shades), vertical ambient groundwater flux (horizontal axes), and biogeochemistry at the three LINX II stream sites: (a and d) NCC, (b and e) PRM, and (c and f) KSL (compare with Figure 8).

addressed by increasing model complexity, for example by adding: (1) an additional term to the mass balance equation for nitrate (equation (4b)) to account for the kinetics of nitrate assimilation [e.g., see *Birgand et al.*, 2007]; (2) a rate equation to the biokinetic model for the evolution of dissolved and/or particulate organic carbon concentration with travel time [*Zarnetske et al.*, 2012]; and (3) additional terms to the mass balance equation for ammonium (equation (4c)) to account for adsorption and assimilation [*Thibodeaux and Mackay*, 2011].

While our model appears to overestimate v_f and $v_{f,Dn}$, estimates of direct denitrification ($v_{f,Dw}$) fall within the range measured by *Mulholland et al.* [2008] during the LINX II studies (Figure 10). It should be stressed that the physical parameters adopted for these simulations, such as stream flow and the hydraulic conductivity of the streambed sediments (see Table 1), were not tailored to the LINX II sites. Thus we do not expect model predictions for $v_{f,Dw}$ to align precisely with the experimentally observed values at NCC, PRM, and KSL (indicated in the figure by large stars).

6.2. Effect of Bed Form Scale

6.2.1. Bed Form Scale and Nitrification Rates

Despite the fact that ripples generate up to 11 times more hyporheic exchange flux than riffle-pool sequences (see section 4), the nitrate uptake velocities predicted for the NCC and KSL sites indicate that more nitrate is produced by riffle-pool sequences than by fluvial ripples (compare light and dark color shades, Figures 8a and 8c). This result can be understood by noting that riffle-pool sequences have relatively long residence times, which in well-oxygenated sediments favor nitrate generation by nitrification. Indeed, comparing F_N curves (predicted by our biokinetic model, Figure 3) with the range of residence times estimated for ripples and riffle-pool sequences (turquoise and green bands of color in the figure) supports the idea that the longer residence times associated with riffle-pools should result in net nitrate generation in NCC and KSL; i.e., the peak in the F_N curve coincides with the range of residence times for water circulating through the riffle-pool sequences. On the other hand, ripples and riffle-pools contribute roughly equally to nitrate generation at PRM (compare light and dark color shades, Figure 8b), consistent with the partial

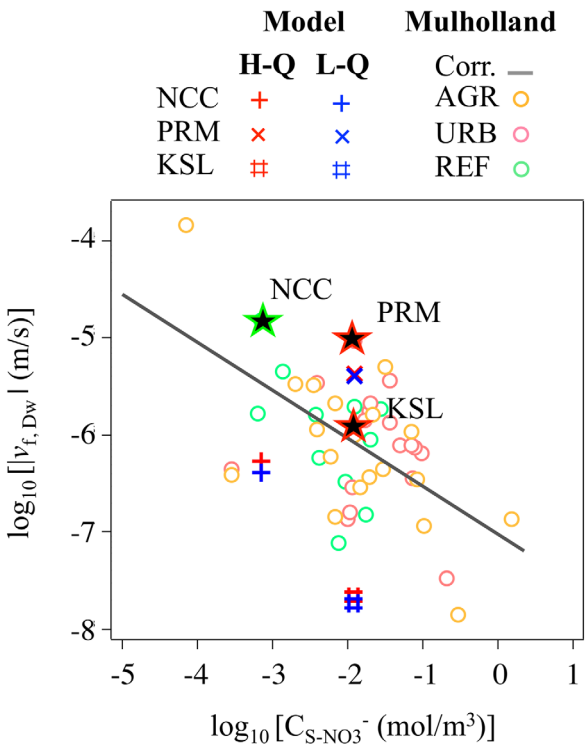

Figure 10. Comparison of model-predicted (blue and red crosses and hatchmarks) and field-measured (colored circles and stars) uptake velocities for the direct denitrification of stream nitrate ($v_{f,Dw}$) plotted against in-stream nitrate concentration ($C_{S-NO_3^-}$). The stars correspond to LINX II sites (NCC, PRM, and KSL) and the black line is an empirical correlation proposed by *Mulholland et al*. [2008] between denitrification velocity and in-stream nitrate concentration proposed. Data reproduced from *Mulholland et al*. [2008].

overlap between the peak of the F_N curve for this site and the RTDs of both ripples and riffle-pool sequences (Figure 3).

6.2.2. Bed Form Scale and Denitrification Rates

Not surprisingly given their longer residence times, riffle-pools also dominate N removal by direct denitrification (Figures 9a–9c) and coupled nitrification-denitrification (Figures 9d–9f). Indeed, according to our model simulations, ripples have virtually no functional role relative to nitrate generation or removal, despite their outsized role in flushing water through the hyporheic zone (Figure 5). It should be noted that bed forms can be net producers of nitrate (i.e., $v_f > 0$) even while they remove N by direct denitrification ($v_{f,Dw} < 0$) and coupled nitrification-denitrification ($v_{f,Dn} < 0$). In such cases, the generation of nitrate by nitrification exceeds the removal of nitrate by one or more pathways.

6.3 Effect of Ambient Groundwater Flow and Stream Discharge

The model-predicted uptake velocities (v_f, $v_{f,Dw}$, and $v_{f,Dn}$) decline sharply with increasing vertical ambient groundwater flow under both gaining and losing conditions (Figures 8 and 9). This occurs because the nitrate uptake velocities are proportional to q_H (see equation (1a)) and q_H declines as the magnitude of q_V is increased (Figure 5). The magnitude of the nitrate uptake velocity is almost always larger at higher stream discharge (compare dark orange and green bars for riffle-pool sequences, and light orange and green bars for ripples, Figures 8 and 9), reflecting the importance of stream discharge as a primary driver of hyporheic exchange flux.

6.4. The Damköhler Number

As noted earlier, the Damköhler Number has been proposed as a master variable for nitrate removal and generation in the hyporheic zone of streams. For example, *Zarnetske et al*. [2012] reported that, across a wide range of randomly selected biokinetic model parameter values, the fractional reduction in nitrate concentration along a single flow path through the hyporheic zone (F_N, see equation (2b)) exhibited a general pattern in which net denitrifying conditions ($F_N < 0$) coincided with $\mathrm{Da} > 1$, whereas net nitrifying conditions ($F_N > 0$) coincided with $\mathrm{Da} < 10$.

To see if a similar pattern applies to our results, we compared model-predicted v_f, $v_{f,Dw}$, and $v_{f,Dn}$ values against their corresponding Da values. As applied here, the Damköhler Number is the ratio of timescales for transport and organic carbon mineralization in the hyporheic zone: $\mathrm{Da} = \tau_T/\tau_R$. The respiration timescale is the ratio of the half-saturation constant for aerobic respiration and the organic carbon mineralization rate ($\tau_R = K_{O_2}^{sat}/R_{min}$). The definition of τ_T, on the other hand, varies by bed form scale. For fluvial ripples, we set τ_T equal to the characteristic transport timescale described earlier for Boano et al.'s advective pumping model (see equation (7d)). For riffle-pool sequences, we first fit Trauth et al.'s RTDs (obtained from particle tracking experiments) to a lognormal distribution, and equated τ_T to the geometric means thus obtained (see supporting information Table S3).

When normalized by the hyporheic exchange flux (q_H), the uptake velocities exhibit a simple functional dependence on Da (Figure 11). For $\mathrm{Da} < 10$, the uptake velocities are a negligible fraction of the hyporheic

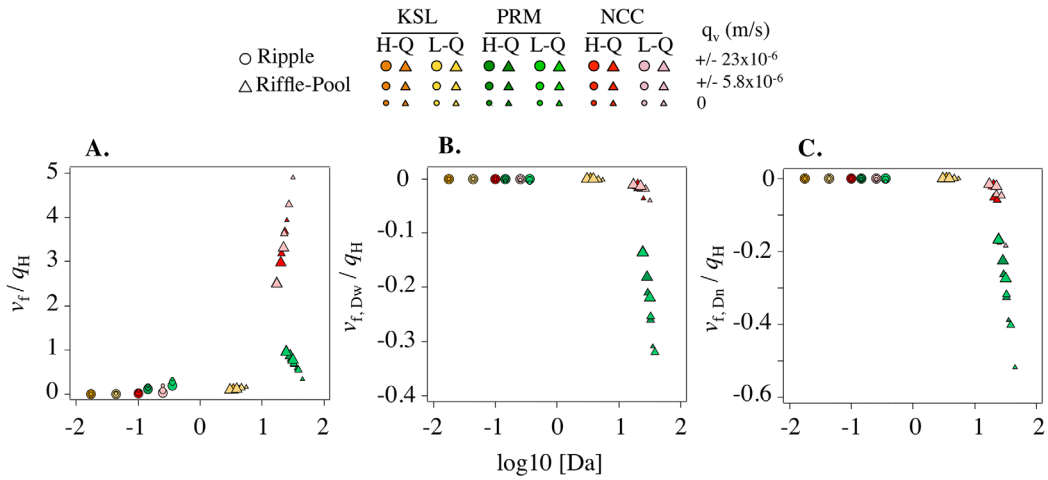

Figure 11. Model predictions for (a) total uptake velocity, (b) uptake velocity for direct denitrification of stream nitrate, and (c) uptake velocity for coupled nitrification-denitrification. When normalized by the hyporheic exchange flux (q_H), the respective uptake velocities exhibit a relatively monotonic dependence on the Damköhler Number (Da, horizontal axis). The circles and triangles denote ripples and riffle-pool sequences, respectively; their color denotes biogeochemical setting (KSL, PRM, NCC); and their size denotes the magnitude of the vertical groundwater flux.

exchange flux (i.e., $v_f/q_H \approx v_{f,Dw}/q_H \approx v_{f,Dn}/q_H \approx 0$). Under such conditions, the sediment bed has no functional role relative to the consumption or generation of nitrate. Above Da = 10, v_f increases with Da, while $v_{f,Dw}$ and $v_{f,Dn}$ decrease with Da. Even at the largest Da tested (~10), direct denitrification and coupled nitrification-denitrification are reaction limited (i.e., $v_{f,Dn}/q_H, v_{f,Dw}/q_H > -1$). Furthermore, nitrate generation by nitrification outcompetes nitrate removal by both direct denitrification and coupled nitrification-denitrification; as a result, v_f is a positive increasing function of Da.

While the results presented in Figure 11 are broadly consistent with those reported by *Zarnetske et al.* [2012], there are several important differences. Zarnetske et al.'s relationship between F_N and Da is relatively diffuse; i.e., the simulations for various random choices of biokinetic model parameters broadly fall into two categories—net denitrifying for Da > 1 and net nitrifying for Da < 10, see Figure 4 in their paper. By contrast, our model-predicted uptake velocities exhibit a nearly monotonic dependence on Da (Figure 11). There are several possible explanations. First, in preparing Figure 11 we normalized our uptake velocities by their corresponding hyporheic exchange fluxes. Any variation in uptake velocity attributable solely to variation in advective mass transfer across the sediment-water interface (e.g., brought on by changing vertical groundwater flux, see Figure 5) has been removed by normalization. Second, as revealed by our earlier PCA analysis (see Figure 2 and section 3.2.2) the various parameters characterizing stream biogeochemistry strongly covary across stream sites. Hence, some of the scatter in Zarnetske et al.'s F_N versus Da relationship may result from treating the biokinetic model parameters as statistically independent—an intrinsic assumption in the Monte Carlo sampling approach these authors employed to generate realizations of F_N. Finally, we have accounted for the in situ generation of ammonium by oxidation of organic matter (ammonification). By contrast, the only source of ammonium in Zarnetske et al.'s simulations is ammonium downwelled from the stream. As a result, our simulations indicate that streambed sediments can be net nitrifying well above Da = 10, whereas nitrification is ammonium-limited at values of Da > 10 in Zarnetske et al.'s simulations.

Our model simulations also suggest that vertical groundwater flux can affect the balance of nitrification and denitrification by altering hyporheic zone RTDs. For example, increasing $|q_V|$ at the PRM site causes the riffle-pool RTD to shift leftward (Figures 6a and 6b), increases the overlap between the F_N peak and the riffle-pool RTD (Figure 3), and thereby increases the net generation of nitrate (i.e., v_f/q_H becomes more positive with increasing $|q_V|$, see green triangles in Figure 11a). The opposite pattern prevails at NCC, where increasing the vertical groundwater flux decreases the overlap between the F_N peak and the riffle-pool RTD (Figure 3) and reduces the net generation of nitrate (v_f/q_H declines with increasing $|q_V|$, red triangles in Figure 11a). These groundwater-induced shifts in the hyporheic zone RTD can also affect denitrification rates.

For example, at PRM the magnitudes of $v_{f,Dw}$ and $v_{f,Dn}$ decline with increasing vertical groundwater flux (green triangles in Figures 11b and 11c). In this case, vertical groundwater flux induces a leftward shift in the RTD, increases the oxygen content of the hyporheic zone, and thereby suppresses both direct denitrification and coupled nitrification-denitrification.

In summary, the results presented in Figure 11 suggest that hyporheic exchange flux and the Damköhler Number exert a primary control on N-cycling in streams. In turn, these two controls on N-cycling are strongly influenced by the vertical groundwater flux. Hyporheic exchange flux controls trafficking of mass and water across the sediment-water interface, and therefore as q_H decreases so does the magnitude of v_f, $v_{f,Dw}$, and $v_{f,Dn}$ (see equation (1a)). All else being equal, increasing the Damköhler Number increases denitrification rates, but can also increase ammonification rates in oxygenated sediments, provided that the rate of ammonification is proportional to the mineralization rate of organic carbon, as assumed here. The biogeochemical setting (as reflected in the choice of biokinetic model parameters) will ultimately determine which of these two opposing processes—increased nitrate production by ammonification and nitrification versus increased nitrate removal by denitrification—dominates as Da increases. Finally, the vertical groundwater flux can affect nitrate processing in at least two ways, by attenuating the hyporheic exchange flux (q_H, see Figure 5) and by inducing a leftward shift in the RTD of water passing through the hyporheic zone (see Figure 6).

7. Scaling-Up to Stream Reaches and Watersheds

In this section, we translate our model-predicted nitrate uptake velocities into the fraction f (unitless) of nitrate load removed or added by hyporheic exchange over a stream reach. From a steady state mass balance over a differential length of stream and assuming uniform flow and neglecting longitudinal dispersion, the following differential equation describes the change in nitrate concentration with downstream distance x associated with N-cycling in the hyporheic zone (all variables defined previously also see notation section).

$$\frac{dC_{S-NO_3^-}}{dx} = \frac{v_f}{d_s U} C_{S-NO_3^-} \tag{11}$$

For a stream reach of length ℓ equation (11) can be integrated to yield the following expression for the evolution of nitrate concentration over the stream reach:

$$\frac{C_{S-NO_3^-}(x=\ell)}{C_{S-NO_3^-}(x=0)} = \exp\frac{v_f \ell}{d_s U} = \exp\frac{v_f}{H_L} \tag{12}$$

The hydraulic loading rate (units m s^{-1}) is defined as $H_L = Q/(W\ell)$ and stream discharge is given by $Q = UWd_s$. If the hyporheic zone is a net sink of nitrate ($v_f < 0$), then the fraction of nitrate load removed (f_R, unitless) from the stream by hyporheic exchange over the stream reach ℓ can be written as follows:

$$f_R = \frac{L_{x=0} - L_{x=\ell}}{L_{x=0}} = 1 - \exp\frac{v_f}{H_L}, v_f < 0 \tag{13}$$

where $L_{x=0}$ and $L_{x=\ell}$ (both units of mol s^{-1}) are loading rate of nitrate at $x = 0$ and $x = \ell$, respectively. Conversely, if the sediments are a net nitrate source ($v_f > 0$), then the fraction of nitrate load added (f_A, unitless) by hyporheic exchange over the stream reach ℓ becomes:

$$f_A = \frac{L_{x=\ell} - L_{x=0}}{L_{x=0}} = \exp\frac{v_f}{H_L} - 1, v_f > 0 \tag{14}$$

Equations (13) and (14) can be consolidated into a single expression for the fraction f (unitless) of nitrate load removed or added by hyporheic exchange:

$$f = \left| 1 - \exp\frac{v_f}{H_L} \right| \tag{15}$$

Equation (15) makes clear that the fate and transport of nitrate in streams depends on the relative strength of biological processes in the hyporheic zone (as quantified by the nitrate uptake velocity v_f) and horizontal transport in the stream (as quantified by hydraulic loading rate, H_L). For a 1 km reach of a 10 m wide stream

with discharge of 7.4 $m^3\ s^{-1}$ (corresponding to our L-Q scenario), under neutral conditions our estimates of v_f imply that stream nitrate load is increased by 0.7%, 0.2%, and 0.03% in NCC, PRM, and KSL, respectively. For our maximum gaining condition ($q_V = +23\times10^{-6} m\ s^{-1}$), these numbers become 0.1%, 0.07%, and 0.005%, respectively.

Scaling such calculations up to an entire watershed (e.g., using a stream network model) [*Wollheim et al.*, 2006] will require estimating q_H and $E(\tau)$ for each stream reach in the network. In the case of ripples, these two quantities can be estimated from equation (7a), and equations (9a) through (9c) given reach-by-reach values for: (1) vertical q_V and horizontal q_U groundwater flux (e.g., based on stream slope, sediment hydraulic conductivity, and estimates of groundwater flux across the sediment-water interface) [*Caruso et al.*, 2016]; (2) stream discharge, width, and depth (e.g., based on stream network model calculations together with appropriate scaling-laws) [see *Mulholland et al.*, 2008]; and (3) the amplitude and wavelength of submerged bed forms responsible for hyporheic exchange. Because small bed forms will likely dominate hyporheic exchange flux (see Figure 5), restricting such calculations to fluvial ripples may be sufficient in cases where nitrate removal is transport limited and therefore $v_f \approx v_{f,MTL} = -q_H$. However, virtually all of our model simulations suggest that, while ripples dominate hyporheic exchange flux, riffle-pool sequences dominate nitrate processing. In this case, it is probably not feasible to conduct reach-by-reach CFD simulations of hyporheic exchange, like those reported by *Trauth et al.* [2013]. Instead, scaling laws [e.g., *Marzadri et al.*, 2010; *Tonina*, 2013] could provide estimates for q_H and $E(\tau)$ at the riffle-pool scale under neutral conditions. Further research is needed to determine how such scaling relationships should be modified to account for ambient groundwater flow.

8. Modeling Limitations and Future Directions

Beyond the limitations already identified with our biokinetic model (see section 6.1.2), there are several aspects of the PASS modeling framework that could be improved moving forward. One potential limitation is that denitrification can only occur once oxygen is depleted along the HZT; i.e., for travel times past the oxic-anoxic transition. Several recent studies suggest that small-scale heterogeneities, or "microzones," within the hyporheic zone can be hotspots for denitrification, even when the bulk sediment is aerobic [*Harvey et al.*, 2013; *Aubeneau et al.*, 2014, 2015a, 2015b; *Briggs*, 2015; *Sawyer*, 2015]. On the other hand, experimental studies of buried macroalgae within sand ripples indicate that this type of heterogeneity may not affect denitrification rates [*Bourke et al.*, 2014]. Microzones may arise from: (1) physical heterogeneities (such as internal porosity within sediment grains) where water parcels become trapped for long periods of time [*Kessler et al.*, 2014]; and (2) spatial variations in reaction rates caused by, for example, variable biofilm density and organic carbon inclusions (e.g., leaf litter or benthic diatoms). Within the HZT framework, physical heterogeneities can be represented by heavy tailed RTD functions, where the "heavy" part of the tail accounts for the trapping of water parcels in immobile zones. Indeed, so-called "mobile-immobile" (MIM) models have been developed to represent reactive mass transport through porous media with slow and fast transport pathways [e.g., *Schumer et al.*, 2001, 2003, 2009]. Presumably, MIM models could be used to represent heterogeneous transport within individual HZTs, along the lines reported in *Sanz-Prat et al.* [2015]. Accounting for biogeochemical heterogeneities, on the other hand, may require adopting a probabilistic, rather than deterministic, description of hyporheic zone reaction fields [e.g., see *Rawlings and Ekerdt*, 2013]. N-cycling can also occur in other components of the stream (i.e., other than the hyporheic zone), such as the stream's water column or in hydraulically disconnected surface storage zones [*Stewart et al.*, 2011].

Finally, while we have focused here on the processing of stream-borne nitrate by hyporheic exchange, it is important to acknowledge that groundwater can also be a significant source of nitrate, particularly in agricultural areas [*Hinkle et al.*, 2001; *Smith et al.*, 2009]. Upwelling of nitrate-contaminated groundwater can affect stream water quality both directly by adding nitrate to the stream, and indirectly by altering features of the hyporheic zone that influence denitrification (as illustrated in this study). Indeed, groundwater upwelling can create conditions favorable for denitrification and the removal of groundwater-borne nitrate, for example, by limiting the depth of aerobic respiration within the streambed and harnessing the denitrification potential of deeper sediments [*Hester et al.*, 2013; *Lansdown et al.*, 2015].

Notation

a	empirical pre-factor in the *Fehlman* [1985] correlation between hyporheic exchange flux, stream velocity, water depth, and bed form geometry (see equation (7c)) (-)
α	normalized in-stream concentration of ammonium by in-stream concentration of oxygen (-)
AM	ammonification
Anammox	anaerobic ammonium oxidation
AR	aerobic respiration
β	normalized in-stream concentration of nitrate by in-stream concentration of oxygen (-)
C_{DOC}	interstitial concentration of dissolved organic carbon (mol m^{-3} s^{-1})
"chemistry"	subsurface biogeochemical reactions that consume and produce nitrate
CDF	cumulative distribution function
CFD	computational fluid dynamics
CH_2O	formaldehyde representing dissolved organic carbon
$C_{HZT-NH_4^+}$	interstitial concentration of ammonium along a HZT (mol m^{-3} s^{-1})
$\hat{C}_{HZT-NH_4^+}$	interstitial concentration of ammonium along a HZT normalized by in-stream concentration of molecular oxygen (-)
$C_{HZT-NO_3^-}$	interstitial concentration of nitrate along a HZT (mol m^{-3} s^{-1})
$\hat{C}_{HZT-NO_3^-}$	interstitial concentration of nitrate normalized by in-stream concentration of molecular oxygen (-)
$\bar{C}_{HZT-NO_3^-}$	normalized "breakthrough" concentration of nitrate in an upwelling zone (see equation (1b)) (-)
C_{HZT-O_2}	interstitial concentration of molecular oxygen along a HZT (mol m^{-3} s^{-1})
$\hat{C}_{HZT-O_2}$	normalized interstitial concentration of molecular oxygen by in-stream concentration of molecular oxygen (-)
CO_2	carbon dioxide (mol m^{-3} s^{-1})
$C_{S-NH_4^+}$	in-stream concentration of ammonium (mol m^{-3} s^{-1})
$C_{S-NO_3^-}$	in-stream concentration of nitrate (mol m^{-3} s^{-1})
C_{S-O_2}	in-stream concentration of oxygen (mol m^{-3} s^{-1})
Da	Damköhler number (-)
DN	denitrification
DNRA	dissimilatory nitrate reduction to ammonium
DOC	dissolved organic carbon
d	approximate depth over which mineralization of organic carbon and respiratory denitrification occur (m)
d_s	depth of stream (m)
δ	relative rates of nitrification and respiration
$\delta(\tau-\tau^*)$	Dirac delta function representation of an RTD with single residence time τ^* (s^{-1})
ER	ecosystem respiration (mol m^{-2} s^{-1})
$E(\tau)$	PDF form of the hyporheic zone RTD (s^{-1})
f	fraction of nitrate load removed or added by hyporheic exchange over a stream reach (-)
f_R	fraction of nitrate load removed from the stream by hyporheic exchange over a stream reach (-)
f_A	fraction of nitrate load added to the stream by hyporheic exchange over a stream reach (-)
F_1	contribution of the upstream flow cell to the ripple RTD (-)
F_2	contribution of the downstream flow cell to the ripple RTD (-)
F_N	fraction of nitrate remaining in HZT after a water parcel travels through the hyporheic zone (-)
F_{RTD}	CDF function
g	gravitational constant (m s^{-2})
γ_{CN}	moles of ammonium released per mole of carbon mineralized (-)
H	height of ripples (m)
H_L	hydraulic loading rate (m s^{-1})
H-Q	high stream discharge scenario
h_0	amplitude of the dynamic pressure head perturbation over a ripple (m)
HZT	hyporheic zone tube

IEZ	interfacial exchange zone
κ	moles of carbon oxidized per mole of nitrate reduced during respiratory denitrification (-)
K_h	hydraulic conductivity (m s^{-1})
KSL	Little Kitten Creek in Kansas; an urban-impacted site selected from LINX II data set
k_{min}	first-order mineralization rate constant (s^{-1})
k_{NI}	nitrification rate constant (m^3 mol^{-1} s^{-1})
$K^{sat}_{NO_3^-}$	half-saturation constant for denitrification (mol m^{-3})
$\hat{K}^{sat}_{NO_3^-}$	half-saturation constant for denitrification normalized by in-stream concentration of oxygen (-)
$K^{inh}_{O_2}$	oxygen inhibition of denitrification (mol m^{-3})
$\hat{K}^{inh}_{O_2}$	oxygen inhibition of denitrification normalized by in-stream concentration of oxygen (-)
$K^{sat}_{O_2}$	half-saturation constant for aerobic respiration (mol m^{-3})
$\hat{K}^{sat}_{O_2}$	half-saturation constant for aerobic respiration normalized by in-stream concentration of oxygen (-)
ℓ	length of a stream reach (m)
$L_{x=0}$	loading rate of nitrate at start of a reach (mol s^{-1})
$L_{x=\ell}$	loading rate of nitrate at length ℓ of a reach (mol s^{-1})
L-Q	low stream discharge scenario
LINX II	second lotic intersite nitrate experiment
λ	wavelength of a ripple (m)
m	empirical exponent in the *Fehlman* [1985] correlation between hyporheic exchange flux, stream velocity, water depth, and bed form geometry (see equation (7c)) (-)
MTL	mass transfer limited
NCC	Cunningham Creek in North Carolina; a reference site selected from the LINX II data set
NI	nitrification
$\{NH_3\}_{OM}$	ammonia associated with organic matter
$^{15}NH_4^+$	^{15}N-labeled ammonium
$^{15}NO_3^-$	^{15}N-labeled nitrate
OM	organic matter
PASS	pumping and streamline segregation model
PDF	probability density function
PRM	Rio Mameyes Tributary in Puerto Rico; an urban-impacted site selected from LINX II data set
Q	stream discharge (m^3 s^{-1})
q_H	hyporheic exchange flux (m s^{-1})
$q_{H,0}$	characteristic hyporheic exchange flux (m s^{-1})
q_U	horizontal component of ambient groundwater flux (m s^{-1})
q_V	vertical component of ambient groundwater flux (m s^{-1})
R_{AM}	rate of ammonification (mol m^{-3} s^{-1})
R_{AR}	rate of aerobic respiration (mol m^{-3} s^{-1})
R_{DN}	rate of denitrification (mol m^{-3} s^{-1})
R_{min}	rate of mineralization of sediment organic matter (mol m^{-3} s^{-1})
R_{NI}	rate of nitrification (mol m^{-3} s^{-1})
RTD	residence time distribution
S	slope of alluvium (-)
τ	travel time through the hyporheic zone (s)
τ_T	characteristic travel time through a bed form by hyporheic exchange (s)
τ^*	a hypothetical travel time through a bed form by hyporheic exchange (s)
$\bar{\tau}$	normalized travel time through the HZT (-)
τ_R	aerobic mineralization time scale (s)
$\hat{\tau}_R$	travel time along a HZT normalized by the mineralization time scale (-)
θ	porosity (-)
$\theta^{inh}_{O_2}$	inhibition coefficient of denitrification with oxygen (-)
U	stream velocity (m s^{-1})
U_{DN}	flux of stream nitrate out of the streambed by direct denitrification (mol m^{-2} s^{-1})

$U_{N_2,Dw}$	flux of nitrogen gas out of the streambed by direct denitrification of stream nitrate (mol m^{-2} s^{-1})
$U_{N_2,Dn}$	flux of nitrogen gas out of the streambed by coupled nitrification-denitrification (mol m^{-2} s^{-1})
$U_{NO_3^-}$	flux of nitrate out of the sediment (mol m^{-2} s^{-1})
v_f	total nitrate uptake velocity (m s^{-1})
v_{fden}	uptake velocity of stream nitrate by direct denitrification as reported by *Mulholland et al.* [2008] (m s^{-1})
$v_{f,Dn}$	uptake velocity for coupled nitrification-denitrification (m s^{-1})
$v_{f,Dw}$	uptake velocity of stream nitrate by direct denitrification (m s^{-1})
$v_{f,MTL}$	total nitrate uptake velocity under MTL conditions (m s^{-1})
W	stream width (m)
x	horizontal coordinate (m)
$\bar{x}$	normalized horizontal coordinate (-)
x_0	starting position of a HZT (m)
$\bar{x}_0$	normalized starting position of a HZT (-)
$x_0^{down-cell}$	location along the sediment-water interface where water first enters the hyporheic zone in the downstream flow cell of ripples (m)
$\bar{x}_0^{down-cell}$	normalized location along the sediment-water interface where water first enters the hyporheic zone in the downstream flow cell of ripples (-)
$x_0^{up-cell}$	location along the sediment-water interface where water first enters the hyporheic zone in the upstream flow cell of ripples (m)
$\bar{x}_0^{up-cell}$	normalized location along the sediment-water interface where water first enters the hyporheic zone in the upstream flow cell of ripples (-)
x_f	final position where water exits the HZT and returns to the stream (m)
$\bar{x}_f$	normalized final position where water exits the HZT and returns to the stream (-)
y	vertical coordinate (m)
$\bar{y}$	normalized vertical coordinate (-)

Acknowledgments
Data presented in Figures (2 and 6), and 10 are either properly cited and referred to in the reference list, or was calculated from data kindly provided by N. Trauth. Financial support was provided by the U.S. National Science Foundation Partnerships for International Research and Education (OISE-1243543) and Australian Research Council (DP130103619). The authors thank Antoine F. Aubeneau, M. Cardenas, and two anonymous reviewers for their constructive feedback on the manuscript, along with A. Mehring, A. McCluskey, M. Stewardson, and A. Kessler for insights and feedback.

References

Ahmerkamp, S., C Winter, F. Janssen, M. M. Kuypers, and M. Holtappels (2015), The impact of bedform migration on benthic oxygen fluxes, *J. Geophys. Res. Biogeosci.*, *120*, 2229–2242, doi:10.1002/2015JG003106.

Askarizadeh, A., et al. (2015), From rain tanks to catchments: Use of low-impact development to address hydrologic symptoms of the urban stream syndrome, *Environ. Sci. Technol.*, *49*(19), 11,264–11,280.

Aubeneau, A. F., B. Hanrahan, D. Bolster, and J, L. Tank (2014), Substrate size and heterogeneity control anomalous transport in small streams, *Geophys. Res. Lett.*, *41*, 8335–8341, doi:10.1002/2014GL061838.

Aubeneau, A. F., J. D. Drummond, R. Schumer, D. Bolster, J. L. Tank, and A. I. Packman (2015a), Effects of benthic and hyporheic reactive transport on breakthrough curves, *Freshwater Sci.*, *34*(1), 301–315.

Aubeneau, A. F., R. L. Martin, D. Bolster, R. Schumer, D. Jerolmack, and A. Packman (2015b), Fractal patterns in riverbed morphology produce fractal scaling of water storage times, *Geophys. Res. Lett.*, *42*, 5309–5315, doi:10.1002/2015GL064155.

Azizian, M., S.B. Grant, A.J. Kessler, P.L.M. Cook, M.A. Rippy, M. Stewardson (2015), Bedforms as biocatalytic filters: A Pumping and Streamline Segregation (PASS) model for nitrate removal in permeable sediments, *Environ. Sci. Technol.*, *49*(18), 10,993–11,002, doi: 10.1021/acs.est.5b01941.

Babamoradi, H., F. Van den Berg, and A. Rinnan (2013), Bootstrap based confidence limits in principal component analysis: A case study, *Chemometr. Intell. Lab. 120*, 97–105.

Beaulieu, J.J., et al. (2011) Nitrous oxide emission from denitrification in stream and river networks, *Proc. Natl. Acad. Sci. U. S. A.*, *108*(1), 214–219.

Berg, P., S. Rysgaard, and B. Thamdrup (2003), Dynamic modeling of early diagnosis and nutrient cycling. A case study in an Arctic marine sediment, *Am. J. Sci.*, *303*, 905–955.

Bernot, M. J., and W. K. Dodds (2005) Nitrogen retention, removal, and saturation in lotic ecosystems, *Ecosystems*, *8*, 442–453.

Bird, R. B., W. E. Stewart, and E. W. Lightfoot (2007), *Transport Phenomena*, John Wiley, New York.

Birgand, F., R. W. Skaggs, G. M. Chescheir, and J. W. Gilliam (2007), Nitrogen removal in streams of agricultural catchments: A literature review, *Crit. Rev. Environ. Sci. Technol. 37*(5) 381–487.

Boano, F., R. Revelli, and L. Ridolfi (2008), Reduction of the hyporheic zone volume due to the stream-aquifer interaction, *Geophys. Res. Let.*, *35*, L09401, doi:10.1029/2008GL033554.

Boano, F., R. Revelli, and L. Ridolfi (2009), Quantifying the impact of groundwater discharge on the surface-subsurface exchange, *Hydrol. Processes*, *23*, 2108–2116.

Boano, F. R., A. Demaria, R. Revelli, and L. Ridolfi (2010), Biogeochemical zonation due to intrameander hyporheic flow, *Water Resour. Res. 46*, W02511, doi:10.1029/2008WR007583.

Boano, F., J. W. Harvey, A. Marion, A. I. Packman, R. Revelli, L. Ridolfi, and A. Worman (2014), Hyporheic flow and transport processes: Mechanisms, models, and biogeochemical implications, *Rev. Geophys.*, *25*, 603–679, doi:10.1002/2012RG000417.

Bohlke, J. K., R. C. Antweiler, J. W. Harvey, A. E. Laursen, L. K. Smith, R. L. Smith, and M. A. Voytek (2009), Multi-scale measurements and modeling of denitrification in streams with varying flow and nitrate concentration in the upper Mississippi River basin, USA, *Biogeochemistry*, *93*, 117–141.

Boulton, A. J., T. Datry, T. Kasahara, M. Mutz, and J. A. Stanford (2010), Ecology and management of the hyporheic zone: Stream-groundwater interactions of running waters and their floodplains, *J. N. Am. Benthol. Soc.*, *29*(1), 26–40.

Bourke, M. F., A. J. Kessler, and P. L. M. Cook (2014), The influence of the buried macroalgae *Ulva lactuca* on denitrification in permeable sediments, *Mar. Ecol. Prog. Ser.*, *498*, 85–94.

Bourke, M. F., P. J. Marriott, R. N. Glud, H. Hassler-Sheetal, M. Kamalanathang, J. Beardall, C. Greening, and P. L. M. Cook (2017), Metabolism in anoxic permeable sediments is dominated by eukaryotic dark fermentation, *Nat. Geosci.*, *10*, 30–35.

Bouwman, A. F., G. Van Drecht, and K. W. Van der Hoek (2005), Global and Regional Surface Nitrogen Balances in Intensive Agricultural Production Systems for the Period 1970-2030, *Pedosphere*, *15*, 137–155.

Briggs, M. A., F. D. Day-Lewis, J. P, Zarnetske, and J. W. Harvey (2015), A physical explanation for the development of redox microzones in hyporheic flow, *Geophys. Res. Lett.*, *42*, 4402–4410, doi:10.1002/2015GL064200.

Buckingham, E. (1914), On physically similar systems; illustration of the use of dimensional equations, *Phys. Rev.*, *4*(4), 345, doi:10.1103/physrev.4.345.

Burgin, A. J., and S. K. Hamilton (2007), Have we overemphasized the role of denitrification in aquatic ecosystems? A review of nitrate removal pathways, *Front. Ecol. Environ.*, *5*(2), 89–96.

Canfield, D. E., A. N. Glazer, and P. G. Falkowski (2010), The evolution and future of earth's nitrogen cycle, *Science*, *330*, 192–196.

Cardenas, M. B. (2008), Surface water-groundwater interface geomorphology leads to scaling of residence times, *Geophys. Res. Lett.*, *35*, L08402, doi:10.1029/2008GL033753.

Cardenas, M. B., and J. L. Wilson (2007a), Exchange across a sediment-water interface with ambient groundwater discharge, *J. Hydrol.*, *346*(3–4), 69–80, doi:10.1016/j.jhydrol.2007.08.019, 69-80.

Cardenas, M. B., and J. L Wilson (2007b), Hydrodynamics of coupled flow above and below a sediment-water interface with triangular bed forms: Underflow case, *Adv. Water. Res.*, *30*(3), 301–313, doi:10.1016/j.advwaters.2006.06.009.

Cardenas, M., J. L. Wilson, and R. Haggerty (2008), Residence time of bedform-driven hyporheic exchange. *Adv. Water Res.*, *31*, 1382–1386.

Carey, R. O., and K. W. Migliaccio (2009), Contribution of wastewater treatment plant effluents to nutrient dynamics in aquatic systems: A review, *Environ. Manage.*, *44*, 205–217.

Caruso, A., Ridolfi, L., Boano, F. (2016), Impact of watershed topography on hyporheic exchange. *Adv. Water Res.*, *94*, 400–411.

Cook, P. L. M., F. Wenzhofer, S. Rysgaard, O. S. Galaktionov, F. J. R. Meysman, B. D. Eyre, J. Cornwell, M. Huettel, and R. N. Glud (2006), Quantification of denitrification in permeable sediments: Insights from a two-dimensional simulation analysis and experimental data, *Limnol. Oceanogr. Methods*, *4*, 294–307.

Coppess, J. (2016), Dead Zones and Drinking Water, Part 1: RCPP and Review, *farmdoc daily*, *6*(6), 37.

Craig, L. S., et al. (2008), Stream restoration strategies for reducing river nitrogen loads, *Front. Ecol. Environ.*, *6*(10), 529–538.

Elliott, A. H., and N. H. Brooks (1997a), Transfer of nonsorbing solutes to a streambed with bed forms: Theory, *Water Resour. Res.*, *33*, 123−136.

Elliott, A. H., and N. H. Brooks (1997b), Transfer of nonsorbing solutes to a streambed with bed forms: Laboratory experiments. *Water Resour. Res.*, *33*, 137−151.

Engelhardt, I., M. Piepenbrink, N. Trauth, S. Stadler, C. Kludt, M. Schulz, C. Schüth, and T. A. Ternes (2011), Comparison of tracer methods to quantify hydrodynamic exchange within the hyporheic zone. *J. Hydrol.*, *400*, 255–266.

Evrard, V., R. N. Glud, and P. L. M. Cook (2012), The kinetics of denitrification in permeable sediments, *Biogeochemistry*, *113*, 563–572, doi:10.1007/s10533-012-9789-x.

Fehlman, H. (1985), Resistance components and velocity distributions of open channel flows over bedforms, MS thesis, Colo. State Univ., Fort Collins.

Feinberg, M., and D. Hildebrandt (1997), Optimal reactor design from a geometric viewpoint—I. Universal properties of the attainable region, *Chem. Eng. Sci.*, *52*(10), 1637–1665.

Fox, A., F. Boano, and S. Arnon (2014), Impact of losing and gaining streamflow conditions on hyporheic exchange fluxes induced by dune-shaped bedforms, *Water Resour. Res.*, *50*, 1895–1907, doi:10.1002/2013WR014668.

Fox, A., G. Laube, C. Schmidt, J. H. Fleckenstein, and S. Arnon (2016), The effect of losing and gaining flow conditions on hyporheic exchange in heterogeneous streambeds, *Water Resour. Res.*, *52*, 7460–7477, doi:10.1002/2016WR018677.

French, C., L. Wu, T. Meixner, D. Haver, J. Kabashima, and W.A. Jury (2006), Modeling nitrogen transport in the Newport Bay/San Diego Creek watershed of Southern California, *Agric. Water Manage.*, *81*, 199–215.

Friedlander, S. K. (2000), Smoke, dust, and haze: Fundamentals of aerosol dynamics, in *Topics in Chemical Engineering*, edited by K. E. Gubbins, Oxford Univ. Press, New York.

Galloway, J. N., et al.(2004), Nitrogen cycles: Past, present, and future, *Biogeochemistry*, *70*, 153–226.

Garcia-Ruiz, R., S. N. Pattinson, and B. A.Whitton (1998), Kinetic parameters of denitrification in a river continuum, *Appl. Environ. Microbiol.*, *64*, 2533–2538.

Gomez-Velez, J. D., and J. W. Harvey (2014), A hydrogeomorphic river network model predicts where and why hyporheic exchange is important in large basins, *Geophys. Res. Lett.*, *41*, 6403–6412, doi:10.1002/2014GL061099.

Gomez-Velez, J. D., J. W. Harvey, M. B. Cardenas, and B. Kiel (2015), Denitrification in the Mississippi River network controlled by flow through river bedforms, *Nat. Geosci.*, *8*, 941–945, doi:10.1038/ngeo2567.

Gooseff, M. N. (2010), Defining hyporheic zones: Advancing our conceptual and operational definitions of where stream water and groundwater meet, *Geogr. Compass*, *4*(8), 945–955, doi:10.1111/j.1749-8198.2010.00364.x.

Grant, S. B., and I. Marusic (2011), Crossing turbulent boundaries: Interfacial flux in environmental flows, *Environ. Sci. Technol.*, *45*, 7107–7113.

Grant, S. B., K. Stolzenbach, M. Azizian, M. J. Stewardson, F. Boano, and L. Bardini (2014), First-order contaminant removal in the hyporheic zone of streams: Physical insights from a simple analytical model, *Environ. Sci. Technol.*, *48*, 11,369–11,378.

Grathwohl, P., et al. (2013), Catchments as reactors: A comprehensive approach for water fluxes and solute turnover, *Environ. Earth Sci.*, *69*, 317–333.

Green, T. R., M. Taniguchi, H. Kooi, J. J. Gurdak, D. M. Allen, K. M. Hiscock, H. Treidel, and A. Aureli (2011), Beneath the surface of global change: Impacts of climate change on groundwater, *J. Hydrol.*, *405*(3), 532–560.

Groffman, P. M., A. M. Dorsey, and P. M. Mayer (2005), N processing within geomorphic structures in urban streams, *J. N. Am. Benthol. Soc.*, *24*(3), 613–625.

Harvey, J. W., J. K. Bohlke, M. A. Voytek, D. Scott, and C. R. Tobias (2013), Hyporheic zone denitrification: Controls on effective reaction depth and contribution to whole-stream mass balance, *Water Resour. Res.*, *49*, 6298–6316, doi:10.1002/wrcr.20492.

Herzog, S. P., C. P. Higgins, and J. E. McCray (2015), Engineered streambeds for induced hyporheic flow: Enhanced removal of nutrients, pathogens, and metals from urban streams, *ASCE J. Environ. Eng.*, *142*(1), 04015053.

Hester, E. T., K. I. Young, and M. A. Widdowson (2013), Mixing of surface and groundwater induced by riverbed dunes: Implications for hyporheic zone definitions and pollutant reactions, *Water Resour. Res.*, *49*, 5221–5237, doi:10.1002/wrcr/20399.

Hill, C. G. (1977), *An Introduction to Chemical Engineering Kinetics and Reactor Design*, chap. 11, John Wiley, New York.

Hinkle, S.R., J. H. Duff, F. J. Triska, A. Laenen, E. B. Gates, K. E. Bencala, D. A. Wents, and S. R. Silva (2001), Linking hyporheic flow and nitrogen cycling near the Willamette River: A large river in Oregon, USA, *J. Hydrol.*, *244*, 157–180.

Holmes, R. M., S. G. Fisher, and N. B. Grimm (1994), Parafluvial nitrogen dynamics in a desert stream ecosystem. *J. N. Am. Benthol. Soc.*, *13*(4), 468–478.

Hu, B. L., L. D. Shen, X. Y. Xu, and P. Zheng (2011), Anaerobic ammonium oxidation (anammox) in different natural ecosystems, *Biochem. Soc. Trans.*, *39*(6), 1811–1816.

Huettel, M., P. Berg, and J. E. Kostka (2014), Benthic exchange and biogeochemical cycling in permeable sediments, *Annu. Rev. Mar. Sci.*, *6*, 23–51.

Jongbloed, A. W., and N. P. Lenis (1998), Environmental concerns about animal manure, *J. Anim. Sci.*, *76*(10), 2641–2648.

Kennedy, C. D., D. P. Genereux, D. R. Corbett, and H. Mitasova (2009), Spatial and temporal dynamics of coupled groundwater and nitrogen fluxes through a streambed in an agricultural watershed, *Water Resour. Res.*, *45*, W09401, doi:10.1029/2008WR007397.

Kessler, A. J., R. N. Glud, M. B. Cardenas, and P. L. M. Cook (2013a), Transport zonation limits coupled nitrification-denitrification in permeable sediments, *Environ. Sci. Technol.*, *47*, 13,404–13,411.

Kessler, A. J., R. N. Glud, M. B. Cardenas, M. Larsen, M. F. Bourke, and P. L. M. Cook (2013b), Quantifying denitrification in rippled permeable sands through combined flume experiments and modeling, *Limnol. Oceanogr.*, *57*, 1217–1232.

Kessler, A. J., M. B. Cardenas, I. R. Santos, and P. L. M. Cook (2014), Enhancement of denitrification in permeable carbonate sediment due to intra-granular porosity: A multi-scale modelling analysis, *Geochim. Cosmochim. Acta*, *141*, 440–453.

Kiel, B. A., and M. B. Cardenas (2014), Lateral hyporheic exchange throughout the Mississippi River network, *Nat. Geosci.*, *7*(6), 413–417.

Lansdown, K., C. M. Heppell, M. Trimmer, A. Binley, A. L. Heathwaite, P. Byrne, and H. Zhang (2015), The interplay between transport and reaction rates as controls on nitrate attenuation in permeable streambned sediments, *J. Geophys. Res. Biogeosci.s*, *120*, 1093–1109, doi: 10.1002/2014JG002874.

Lansdown, K., B. A. McKew, C. Whitby, C. M. Heppell, A. J. Dumbrell, A. Binley, L. Olde, and M. Trimmer (2016), Importance and controls of anaerobic ammonium oxidation influenced by riverbed geology, *Nat. Geosci.*, *9*, 357–360, doi:10.1038/ngeo2684.

Leeder, M. R. (2012), *Sedimentology: Process and Product*, Springer, London.

Levenspiel, O. (1972), *Chemical Reaction Engineering*, John Wiley, New York.

Marzadri, A., D. Tonina, A. Bellin, G. Vignoli, and M. Tubino (2010), Semianalytical analysis of hyporheic flow induced by alternate bars, *Water Resour. Res.*, *46*, W07531, doi:10.1029/2009WR008285.

Mazadri, A., D. Tonina, and A. Bellin (2011), A semi-analytical three-dimensional process-based model for hyporheic nitrogen dynamics in gravel bed rivers, *Water Resour. Res.*, *47*, W11518, doi:10.1029/2011WR010583.

Marzadri, A., D. Tonina, A. Bellin, and A. Valli (2015), Mixing interfaces, fluxes, residence times and redox conditions of the hyporheic zones induced by dune-like bedforms and groundwater flows, *Adv. Water Resour.*, *88*, 139–151, doi: 10.1016/j.advwatres.2015.12.014.

McClain, M. E., et al. (2003), Biogeochemical hot spots and hot moments at the interface of terrestrial and aquatic ecosystems, *Ecosystems*, *6*, 301–331.

McCluskey, A. H., S. B. Grant, M. J. Stewardson (2016), Flipping the thin film model: Mass transfer by hyporheoc exchange in gainng and losing streams, *Water. Resour. Res.*, *52*, 7806–7818, doi:10.1002/2016WR018972

Meysman, F. J. R., O. S. Galaktionov, P. L. M Cook, F. J. J. G. Janssen, M. Huettel, and J. J. Middelburg (2006a), Quantifying biologically and physically induced flow and tracer dynamics in permeable sediments, *Biogeosci. Discuss.*, *3*(6), 1809–1858.

Meysman, F. J. R., O. S. Galaktionov, B. Gribsholt, and J. J. Middelburg (2006b), Bioirrigation in permeable sediments: Advective pore water transport induced by burrow ventilation, *Limnol. Oceanogr.*, *51*, 142–156.

Morée, A. L., A. H. W. Beusen, A. F. Bouwman, and W. J. Willems (2013), Exploring global nitrogen and phosphorus flows in urban wastes during the twentieth century, *Global Biogeochem. Cycles*, *27*, 836–846, doi:10.1002/gbc.20072.

Mulholland, P. J., J. L. Tank, D. M. Sanzone, W. M. Wollheim, B. J. Peterson, J. R. Webster, and J. L. Meyer (2000), Nitrogen cycling in a forest stream determined by a 15N tracer addition, *Ecol. Monogr.*, *70*(3), 471–493.

Mulholland, P. J., et al. (2008), Stream denitrification across biomes and its response to anthropogenic nitrate loading, *Nature*, *452*, 202–205.

Mulholland, P. J., et al. (2009), Nitrate removal in stream ecosystems measured by 15N addition experiments: Denitrification, *Limnol. Oceanogr.*, *54*(3), 666–680.

National Environmental Research Institute (2004), A model set-up for an oxygen and nutrient flux model for Aarhus Bay (Denmark), *NERI Tech. Rep*. 483, Denmark.

Nielsen, L. P., and N. P. Sloth (1994), Denitrification, nitrification and nitrogen assimilation in photosynthetic microbial mats, in *Microbial Mats: Structure, Development and Environmental Significance*, edited by L. J. Stal, and P. Caumette, *NATO ASI Ser*., vol. 35, pp. 319–324, Springer, New York.

Packman, A. I., N. H. Brooks, and J. J. Morgan (2000), A physiochemical model for colloid exchange between a stream and a sand streambed with bed forms, *Water Resour. Res.*, *36*, 2351–2361, doi:10.1029/2000WR900059.

Peres-Neto, P. R., D. A. Jackson, K. M. Somers (2005), How many principal components? Stopping rules for determining the number of non-trivial axes revisited, *Comput. Stat. Data Anal. 49*, 974–997.

Peterson, B. J., et al. (2001), Control of nitrogen export from watersheds by headwater streams, *Science*, *292*(5514), 86–90.

Pett, R. J. (1989), Kinetics of microbial mineralization of organic carbon from detrital Skeletonema costatum cells, *Mar. Ecol. Prog. Se.*, *52*(2), 123–128.

Powlson, D. S., T. M. Addiscott, N. Benjamin, K. G. Cassman, and T. M. de Kok (2008), When does nitrate become a risk for humans?, *J. Environ. Qual.*, *37*, 291–295.

Rawlings, J. B., and J. G. Ekerdt (2013), *Chemical Reactor Analysis and Design Fundamentals*, chap. 8, Nob Hill Publ., Madison, Wis.

Ribot, M., E. Martí, D. von Schiller, F. Sabater, H. Daims, and T. J. Battin (2012), Nitrogen processing and the role of epilithic biofilms downstream of a wastewater treatment plant, *Freshwater Sci.*, *31*(4), 1057–1069.

Rippy, M. A., A. Deletic, J. Black, R. Aryal, J.-L. Lampard, J. Y.M. Tang, D. McCarthy, P. Kolotelo, J. Sidhu, and W. Gernjak (2017), Pesticide occurrence and spatiotemporal variability in urban run-off across Australia, *Water Res.*, *115*, 245–255.

Rode, M., M. Hartwig, D. Wagenschein, T. Kebede, and D. Borchardt (2015), The importance of hyporheic zone processes on ecological functioning and solute transport of streams and rivers, in *Ecosystem Services and River Basin Ecohydrology*, edited by L. Chicharo, pp. 57–82, Springer, Netherlands.

Runkel, R. L. (2007), Toward the transport-based analysis of nutrient spiraling and uptake in streams, *Limnol. Oceanogr. Methods*, *5*, 50–62.

Rutherford, J. C., G. J. Latimer, and R. K. Smith (1993), Bedform mobility and benthic oxygen uptake, *Water Res.*, *27*(10), 1545–1558.

Rutherford, J. C., J. D. Boyle, A. H. Elliott, T. V. J. Hatherell, and T. W. Chiu (1995), Modeling benthic oxygen uptake by pumping, *ASCE J. Environ. Eng.*, *121*(1), 7216.

Sanz-Prat, A., C. Lu, M. Finkel, and O. Cirpka (2015), On the validity of travel-time based nonlinear bioreactive transport models in steady-state flow, *J. Contam. Hydrol.*, *175*, 26–43, doi:10.1016/j.jconhyd.2015.02.003.

Sawyer, A. H. (2015), Enhanced removal of groundwater-borne nitrate in heterogeneous aquatic sediments, *Geophys. Res. Lett.*, *42*, 403–410, doi:10.1002/2014GL062234.

Schmidt, C., M. Bayer-Raich, and M. Schirmer (2006), Characterization of spatial heterogeneity of groundwater-stream water interactions using multiple depth streambed temperature measurements at the reach scale, *Hydrol. Earth Syst. Sci.*, *10*(6), 849–859.

Schumer R., D. A. Benson, M. M. Meerschaert, and S. W. Wheatcraft (2001), Eulerian derivation of the fractional advection-dispersion equation, *J. Contam. Hydrol.*, *48*, 69–88.

Schumer, R., D. A. Benson, M. M. Meerschaert, and B. Baeumer (2003), Fractal mobile/immobile solute transport, *Water Resour. Res.*, *39*(10), 1296, doi:10.1029/2003WR002141.

Schumer R., M. M. Meerschaert, and B. Baeumer (2009) Fractional advection-dispersion equations for modeling transport of the Earth surface, *J. Geophys. Res.*, *114*, F00A07, doi:10.1029/2008JF001246.

Seitzinger, S., J. A. Harrison, J. K. Bohlke, A.F. Bouwman, R. Lowrance, B. Peterson, C. Tobias, and G. Van Drecht (2006), Denitrification across Landscapes and Waterscapes: A Synthesis, *Ecol. Appl.*, *16*, 2064–2090.

Smith, V. H., G. D. Tilman, and J. C. Nekola (1999), Eutrophication: Impacts of excess nutrient inputs on freshwater, marine, and terrestrial ecosystems, *Environ. Pollut.*, *100*, 179–196.

Smith, J. W. N., B. W. Surridge, T. H. Haxton, and D. N. Lerner (2009), Pollutant attenuation at the groundwater–surface water interface: A classification scheme and statistical analysis using national-scale nitrate data, *J. Hydrol.*, *369*(3), 392–402.

Stewart, R. J., W. M. Wollheim, M. N. Gooseff, M. A. Briggs, J. M. Jacobs, B. J. Peterson, and C. S. Hopkinson (2011), Separation of river network-scale nitrogen removal among the main channel and two transient storage compartments, *Water Resour. Res.*, *47*, W00J10, doi:10.1029/2010WR009896.

Stream Solute Workshop (1990), Concepts and methods for assessing solute dynamics in stream ecosystem, *J. N. Am. Benthol. Soc.*, *9*, 95–119.

Taylor, P. G., and A. R. Townsend (2010), Stoichiometric control of organic carbon–nitrate relationships from soils to the sea, *Nature*, *464*(7292), 1178–1181.

Thibodeaux, L. J., and J. D. Boyle (1987) Bedform-generated convective transport in bottom sediment, *Nature*, *325*(22) 341–343.

Thibodeaux, L. J., and D. Mackay (2011), *Handbook of Chemical Mass Transport in the Environment*, CRC Press, Boca Raton, Fla.

Tonina, D., A. Marzadri, and A. Bellin (2015), Benthic uptake rate due to hyporheic exchange: The effects of streambed morphology for constant and sinusoidally varying nutrient loads, *Water*, *7*(2), 398–419, doi:10.3390/w7020398.

Trauth, N., C. Schmidth, U. Maier, M. Wieweg, and J. H. Fleckenstein (2013), Coupled 3-D stream flow and hyporheic flow model under varying stream and ambient groundwater flow conditions in a pool-riffle system, *Water Resour. Res.*, *49*, 5834–5850, doi:10.1002/wrcr.20442.

Trauth, N., J. C. Schmidt, M. Vieweg, U. Maier, and J. H. Fleckenstein (2014), Hyporheic transport and biogeochemical reactions in pool-riffle systems under varying ambient groundwater flow conditions, *J. Geophys. Res. Biogeosci.*, *119*, 910–928, doi:10.1002/2013JG002586.

Vaughn, C. C., and C. C. Hakenkamp (2001) The functional role of burrowing bivlaves in freshwater ecosystems, *Freshwater Biol.*, *46*, 1431.

Van Cappellen, P., and Y. Wang (1996), Cycling of iron and manganese in surface sediments, A general theory for the coupled transport and reaction of carbon oxygen, nitrogen, sulfur, iron, and manganese, *Am. J. Sci.*, *296*(3) 197–243, doi:10.2475/ajs.296.3.197.

Walsh, C. J., A. H. Roy, J. W. Feminella, P. D. Cottingham, P. M. Groffman, and R. P. Morgan II (2005), The urban stream syndrome: Current knowledge and the search for a cure, *J. N. Am. Benthol. Soc.*, *24*(3), 706–723.

Wollheim, W. M., C. J. Vorosmarty, B. J. Peterson, S. P Seitzinger, and C. S. Hopkinson (2006), Relationship between river size and nutrient removal, *Geophys. Res. Lett.*, *33*, L06410, doi:10.1029/2006GL025845.

Wondzell, S. M. (2015), Groundwater–surface-water interactions: perspectives on the development of the science over the last 20 years, *Freshwater Sci.*, *34*(1), 368–376.

Yang, Y. S., and L. Wang (2010), A review of modeling tools for implementation of the EU Water Framework Directive in handling diffuse water pollution, *Water Resour. Manage. 24*, 1819–1843.

Zarnetske, J. P., R. Haggerty, S. M. Wondzell, and M. A. Baker (2011), Dynamics of nitrate production and removal as a function of residence time in the hyporheic zone, *J. Geophys. Res.*, *116*, G01025, doi:10.1029/2010JG001356.

Zarnetske, J. P., R. Haggerty, S. M. Wondzell, V. A. Bokil, and R. Gonzalez-Pinzon (2012), Coupled transport and reaction kinetics control the nitrate source-sink function of hyporheic zones, *Water Resour. Res.*, *48*, W11508, doi:10.1029/2012WR011894.

Zarnetske, J. P., R. Haggerty, and S. M. Wondzell (2015), Coupling multiscale observations to evaluate hyporheic nitrate removal at the reach scale, *Freshwater Sci.*, *34*(1), 172–186.